THE UNIVERSITY OF MANITOBA

DURABILITY OF GFRP PINS AND REINFORCEMENT IN HERITAGE CONCRETE STRUCTURES

By

Aaron Kroeker

A Thesis Submitted to the
Faculty of Graduate Studies in partial fulfillment
of the requirements for the
Degree of Masters of Science

DEPARTMENT OF CIVIL ENGINEERING
UNIVERSITY OF MANITOBA
AUGUST 2005

THE UNIVERSITY OF MANITOBA

FACULTY OF GRADUATE STUDIES

*****

COPYRIGHT PERMISSION

"Durability of GFRP Pins and Reinforcement in Heritage Concrete Structures"

BY

Aaron Kroeker

A Thesis/Practicum submitted to the Faculty of Graduate Studies of The University of Manitoba in partial fulfillment of the requirement of the degree

Of

MASTER OF SCIENCE

ACKNOWLEDGEMENTS

I would like to take this opportunity to express my sincere thanks and appreciation to my Advisor, Dr. Aftab Mufti, for his technical support, guidance, and encouragement throughout the course of this project. I would also like to thank Dr. Maria Onofrei, consultant to ISIS Canada, for her technical expertise.

The author would like to thank the National and International Memorials Canada Remembers Division, Veterans Affairs Canada (VAC) and Heritage Conservation Directorate (HCD), Public Works and Government Services Canada and ISIS Canada for jointly funding the research described in this report. The author also gratefully acknowledges the support of Specialty Construction Products Ltd., Pultrall Inc. and Larsen Memorials.

In addition, the author would like to acknowledge the technical assistance of Mr. Moray McVey, Mr. Grant Whiteside, Ms. Evangeline Rivera and Mr. Chad Klowak for their assistance in the laboratory and field research related to this project. Also, the support provided by the ISIS Canada administrative staff, and in particular, Ms. Nancy Fehr for the editing services she provided to assist in the timely completion of this thesis is gratefully acknowledged.

ABSTRACT

The rapid deterioration of military grave markers at Brookside Cemetery has exposed a need for a more durable marker mounting assembly, which is able to withstand severe freeze/thaw cycles like those experienced in Winnipeg, Manitoba. Three marker mounting methods have been developed incorporating high strength concrete, corrosion resistant Glass Fibre Reinforced Polymers, and marker mounting assemblies which are less likely to initiate cracking and accelerate deterioration. Each marker mounting assembly was evaluated based on mounting pin pullout tests and lateral tests. These tests have been performed on full-scale specimens after aggressive conditioning in an environmental chamber. Furthermore, steel and GFRP reinforced support beam sections have been evaluated for bending and shear capacity after exposure to simultaneous freeze/thaw conditioning and sustained loading.

TABLE OF CONTENTS

1. INTRODUCTION ---------- 1

   1.1 Brookside Cemetery ---------- 3

   1.2 Background ---------- 3

2. OBJECTIVE AND SCOPE ---------- 4

3. ENVIRONMENTAL EFFECTS ON GFRP REINFORCED CONCRETE ---------- 5

   3.1 GFRPs and Sources of Degradation ---------- 5

   3.2 Sustained Loading on GFRPs ---------- 6

   3.3 Implications of Using GFRP Reinforcement in Concrete Structures ------- 7

4. BOND BEHAVIOUR ---------- 9

   4.1 Introduction ---------- 9

   4.2 Theoretical Bond – Slip Relationship ---------- 10

   4.3 Bond Effects of GFRP Bars ---------- 12

5. EXPERIMENTAL PROGRAM ---------- 13

   5.1 Test Variables ---------- 14

   5.2 Mounting Methods ---------- 14

   5.3 Test Materials ---------- 16

5.4 Reinforced Concrete Support Beam Design ---- 17

5.5 Reinforced Concrete Beam Specimen Preparation ---- 26

5.5.1 Pullout specimen preparation ---- 27

5.5.2 Lateral test specimen preparation ---- 29

5.5.3 Shear and bending test specimen preparation ---- 31

5.6 Exposure Conditions ---- 31

5.6.1 Temperature cycle profiles ---- 32

5.6.2 Specimen saturation ---- 34

5.6.3 Sustained stresses on support beam specimens ---- 35

5.6.3.1 Support beam specimens tested in bending ---- 36

5.6.3.2 Support beams tested in shear ---- 39

5.7 Mechanical Tests ---- 42

5.7.1 Pullout test ---- 42

5.7.2 Lateral test ---- 44

5.7.3 Shear test ---- 45

5.7.2 Bending test ---- 46

6. RESULTS AND DISCUSSION ---- 50

6.1 Pullout Test ---- 50

6.1.1 Threaded stainless steel rods ---- 50

6.1.2 GFRP rods ---- 54

6.2 Lateral Test ---- 58

6.3 Shear Test---------- 67

6.4 Bending Test---------- 72

7. CONCLUSIONS AND RECOMMENDATIONS---------- 76

References---------- 80

Appendix A. Shear Test Strain Gauge Graphs---------- 83

Appendix B. Bending Test Strain Gauge Graphs---------- 86

LIST OF TABLES

Table 1. Test variables considered in the experimental program ---------- 14

Table 2. Mechanical Properties of GFRP V-ROD™ Bars ---------- 16

Table 3. Concrete properties for each concrete batch used in casting test specimens ---------- 28

Table 4. Lateral test specimens ---------- 29

Table 5. Summarized pullout test results for stainless steel specimens --------- 51

Table 6. Summarized pullout test results for GFRP specimens ---------- 55

Table 7. Lateral test results for markers attached with stainless steel pins ----- 59

Table 8. Lateral test results for markers attached with GFRP pins ---------- 59

Table 9. Lateral test results for markers attached by the pocket method -------- 60

Table10. Lateral test results for markers attached by the bumper method------- 60

Table 11. Shear test specimens ---------- 67

Table 12. Shear test results ---------- 68

Table 13. Bending test results ---------- 72

LIST OF FIGURES

Figure 1. Longitudinal cracking along beam ---------- 2

Figure 2. Cracking originating at slot ---------- 2

Figure 3. Severe longitudinal cracking ---------- 2

Figure 4. Corrosion induced spalling of concrete ---------- 2

Figure 5. Theoretical Bond Stress – Bond Slip Relationship ---------- 11

Figure 6. Support beam cross section ---------- 14

Figure 7. Marker mounting assemblies to be evaluated ---------- 15

Figure 8. Shear and bending moment diagrams for 7.32 m beam ---------- 18

Figure 9. Schematic of marker mounting pins embedded in epoxy ---------- 28

Figure 10. Schematic of pinned lateral test specimen preparation ---------- 30

Figure 11. Lateral test specimens prior to attaching granite markers ---------- 31

Figure 12. Pullout specimens in environmental chamber ---------- 32

Figure 13. Freeze and thaw profile for test specimens ---------- 33

Figure 14. Specimens immersed in Ca $(OH)_2$ bath ---------- 35

Figure 15. Self reacting sustained bending stress apparatus outside environmental chamber ---------- 36

Figure 16. Schematic of bending stress apparatus ---------- 37

Figure 17. Bending apparatus equivalent to cantilever support ---------- 37

Figure 18. Bending moment diagram for bending specimens ---------- 37

Figure 19. Compressive failure of concrete due to force couple over support ---- 38

Figure 20. Sustained shear stress apparatus inside environmental chamber ----- 39

Figure 21. Schematic of sustained shear stress apparatus ---------- 39

Figure 22. Shear stress apparatus equivalent to four point loading setup --------- 40

Figure 23. Shear stress diagram for shear test specimens ---------- 40

Figure 24. Flexural cracks, *a/d* = 1.6 ---------- 42

Figure 25. Laboratory setup for the pullout test ---------- 43

Figure 26. Steel sleeves fixed to GFRP rods ---------- 44

Figure 27. Laboratory lateral load test setup ---------- 45

Figure 28. Shear test setup ---------- 46

Figure 29. Cantilever bending test setup ---------- 47

Figure 30. Force couple in cantilever support causing crushing of concrete ------48

Figure 31. Simply supported bending test setup ----------49

Figure 32. Stainless steel pullout specimen after typical yielding failure ----------52

Figure 33. Load-slip behaviour of stainless steel pullout specimens ----------53

Figure 34. Typical slippage observed at epoxy – concrete interface ----------54

Figure 35. Typical slippage failure of GFRP pullout specimens----------56

Figure 36. Pullout load – slip performance of GFRP pullout specimens----------57

Figure 37. Typical slippage observed at the GFRP – epoxy interface----------58

Figure 38. Failed pinned specimens----------61

Figure 39. Failed pocket specimen ----------62

Figure 40. Failed pocket specimen ----------62

Figure 41. Typical lateral load – marker deflection behaviour ----------64

Figure 42. Barre granite marker pinned with 305 mm GFRP pins----------65

Figure 43. Barre granite marker virtually undamaged ----------66

Figure 44. Standstead granite marker ----------66

Figure 45. Shear test results---------- 68

Figure 46. Typical failed shear test specimen ---------- 69

Figure 47. Load – deflection behaviour of shear test specimens ---------- 71

Figure 48. Bending test results---------- 73

Figure 49. Typical bending test failed specimen ---------- 74

Figure 50. Load – deflection behaviour for bending test specimens---------- 75

1. INTRODUCTION

Over the last twenty years the rapid deterioration of veterans grave markers has been a growing concern for the National and International Memorials Canada Remembers Division, Veterans Affairs Canada (VAC) and Heritage Conservation Directorate (HCD), Public Works and Government Services Canada. The grave marker mounting assemblies and the support beams that are currently used are susceptible to severe cracking, spalling, and corrosion of steel reinforcement. This degradation is especially prevalent in Brookside Cemetery; Canada's second largest veterans cemetery located in Winnipeg, Manitoba.

The harsh climate in Winnipeg is one of the key factors behind the rapid degradation of these members. Temperatures vary as much as 60 degrees C between the summer and winter months. These extreme freeze/thaw cycles combined with moisture infiltration facilitate the corrosion of steel reinforcement and crack propagation - likely the most significant factors contributing to rapid degradation.

Another reason for the rapid deterioration is the method used to anchor the grave markers to the support beam. A common method currently used at Brookside Cemetery is to cut a rectangular slot directly into the cured concrete support beam and place the grave markers inside this slot. Cutting directly into cured concrete in this fashion can easily initiate crack development. As can be seen in Figures 1 through 3, the majority of the cracking has started at or near the slot. Once cracking has occurred, water seeps into cracks and causes the steel reinforcement to corrode, increasing its volume and causing spalling. Examples of the spalling of the support beam can be seen in Figure 4.

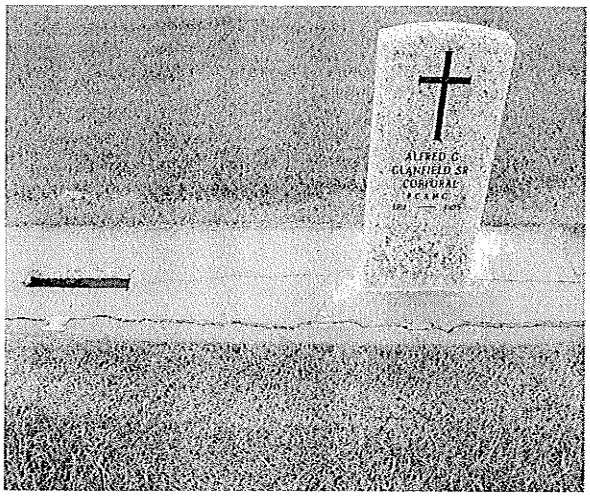

Figure 1. Longitudinal cracking along beam.

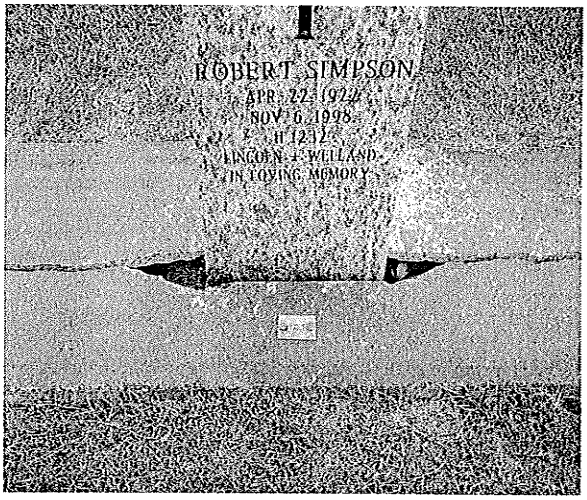

Figure 2. Cracking originating at slot.

Figure 3. Severe longitudinal cracking.

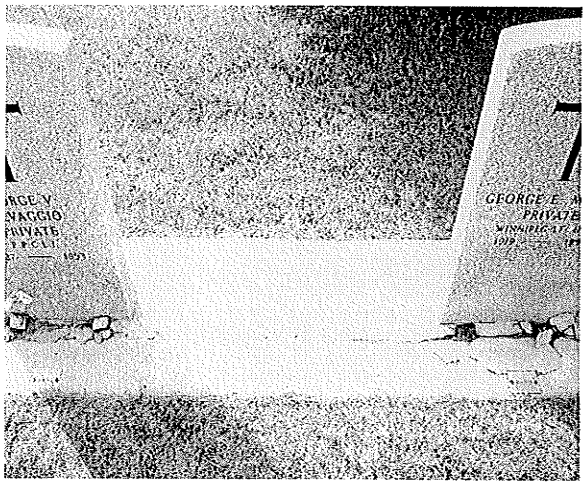

Figure 4. Corrosion induced spalling of concrete.

In order to address these durability issues, the design of the structural system has been altered to incorporate high strength concrete (which has more resistance to cracking), corrosion resistant glass fibre reinforced polymer (GFRP) reinforcement, and marker mounting assemblies that are less likely to initiate cracking.

1.1 Brookside Cemetery

In 1877 the City of Winnipeg purchased 160 acres of land, which was to be used for a new cemetery named Brookside Cemetery. After 125 years of continuous operation, Brookside Cemetery is the final resting place of over 97,000 people. The Field of Honor, the name given to the military portion of Brookside Cemetery, is the oldest and second largest military burial site in Canada. Almost 10,000 Canadian veterans from World War I, World War II, the Korean War, and the Vietnam War are buried here.

1.2 Background

In early 1990, after significant deterioration of veterans' monuments had occurred at Brookside Cemetery, a new design incorporating pre-stressed hollow core concrete floor beams was developed as a pilot project. Shortly after the new design was implemented – and in some cases in as little as a year, cracking and rapid deterioration was apparent. By 1999, a large number of the hollow core support beams had failed, about 5% of the military monuments and about 40% of the civilian monuments in the cemetery [Kowalchuck, 1999; Weaver, 2002].

In 2002, it was suggested that different methods of attaching the marker to the support beam should be investigated [Weaver, 2002]. Preliminary results from a series of freeze/thaw tests carried out at the University of Manitoba under the supervision of Intelligent Sensing of Innovative Structures (ISIS) Canada, indicated that stainless steel and glass fibre reinforced polymer (GFRP) rods fixed with Hilti 500 epoxy or Sika -212 grout are promising marker anchor methods that warrant further investigation [Mufti et al, 2003].

2. OBJECTIVE AND SCOPE

The objective of this study was to assist in developing a marker mounting assembly, which is durable and economical, by evaluating the long-term performance and behaviour of various assemblies after simulated environmental conditioning in the laboratory. The marker mounting assemblies were evaluated through a series of mechanical tests, which were designed to gain an understanding of the structural behaviour of each type of assembly, and the effects that exposure to freeze/thaw cycles have on performance. In addition, this study was also designed to evaluate the durability of a new support beam design and compare the performance of beams reinforced with corrosion resistant GFRP materials, to beams reinforced with traditional steel reinforcement.

This study was intended to address the durability issues found at Brookside Cemetery in Winnipeg, Manitoba, while also being able to apply the findings to other veterans' cemeteries throughout Canada. Furthermore, the results of this study will be used by Veterans Affairs Canada to help make recommendations regarding future rehabilitation and new construction of all veterans' monuments.

3. ENVIRONMENTAL EFFECTS ON GFRP REINFORCED CONCRETE

Over the last 20 years, corrosion-resistant glass fibre reinforced polymers (GFRPs) have been introduced as an alternative material to steel reinforcement, largely to eliminate corrosion-based degradation. Extensive research has been conducted on the physical, mechanical and short-term properties of GFRP materials, however, one of the largest obstacles preventing the extensive use of GFRPs in construction is a lack of long term durability data. Researchers are now addressing this issue, and the long-term durability of GFRP materials is being investigated under various service environments. In order to ensure the success of GFRP materials, they must demonstrate good long-term durability in order to offset the original high cost of the material by an improved structure service life and reduced maintenance costs.

3.1 GFRPs and Sources of Degradation

GFRPs are composite materials composed of a polymer matrix (resin) and reinforcing glass fibres. The resin protects the fibres from mechanical abrasion and harmful environments, while allowing stress to be carried and transferred between individual fibres. It has been shown that the durability of FRP materials is dependant mainly upon the type of matrix material used, as it is this component that is primarily exposed to the environments [Hullat et al, 2002].

Some environmental conditions that have been shown to have a negative effect on the strength of reinforcing glass fibres either individually or in combination include: exposure to alkaline environments (concrete pore water), exposure to saline (chloride) environments, high temperature, UV exposure (for externally applied GFRP reinforcement), wet/dry cycles, moisture exposure, and exposure to freeze/ thaw cycles [Umoto, 2001; Liao et al, 1998; Stone et al, 2002; Melvar et al, 2002]. Combinations of these exposure conditions have been shown to produce more severe degradation.

3.2 Sustained Loading on GFRPs

The most serious degradation occurs when the resin matrix fails to protect the reinforcing glass fibres, leaving the fibres directly exposed to damaging environments. Abrasion or cracking of matrix material is a common way for fibres to become exposed. Resin cracking frequently occurs in GFRP materials when they are subjected to large sustained stresses; the larger the sustained stress, the higher the potential for these cracks to form. Once cracks have formed, the resin matrix can be penetrated quickly and the fibres become exposed and vulnerable. Previous research shows that GFRP bars exposed to harsh environments under sustained loading degrade much more rapidly than unstressed bars exposed to the same conditions [Almusallam, 2002; Helbling, 2002]. For this reason the Canadian Highway Bridge Design Code limits the sustained stress on GFRP bars to 20% of their ultimate capacity (CHBDC, 2000).

Extensive research has been undertaken in the last ten years to investigate the durability of GFRP bars under sustained loads and 'accelerated aging conditions'. For example, to simulate the alkaline environment found in the porewater in concrete, researchers typically submerge FRP bars in strong alkaline solutions called simulated porewater solutions (SPSs). These solutions generally have exceptionally high, constant pH often at elevated temperatures. Degradation under these 'accelerated' conditions is often severe and specimens often fail under the applied sustained loads before their exposure time is complete [Rahman et al, 1996; Sen, et al, 2002; Greenwood, 2002]. It is well known that the volume of solution in cured concrete is quite small, and after the initial curing period, the number of free hydroxide ions in solution decreases dramatically. This results in a sharp decline in the pH of concrete, and thus a corresponding decline in the rate of degradation of FRPs. This is not considered in accelerated testing.

Furthermore, there is some question as to the validity of such accelerated methods and whether this extreme degradation would ever occur to GFRP bars embedded in concrete. Although it is always important for researchers to address worst case conditions, in the case of evaluating FRPs in concrete, the results obtained from some accelerated tests using SPSs may be so conservative as to be meaningless. It follows that the only method of accurately evaluating the real-time durability of FRP materials in concrete, is to include FRP specimens embedded in concrete to any test methodology. B. Benmokrane [Benmokrane et al, 1998], a leader in durability testing, stated that for a realistic evaluation of the durability of FRP rebar in concrete, it is necessary to do the tests on specimens embedded in concrete.

3.3 Implications of Using GFRP Reinforcement in Concrete Structures

As previously discussed, GFRP materials may be subject to degradation when exposed to an alkaline environment, such as when they are used as reinforcement for concrete members. This degradation, however, is now believed to take place over a very long period of time. In a recent study, core samples were taken from five GFRP reinforced demonstration structures ranging between 5 and 8 years of age to investigate elapse-time degradation that occurs in structures under normal service load conditions. Four research teams independently performed a microscopic evaluation on the GFRP bars extracted from the cores, and each team concluded that there were no signs of any degradation within the GFRP reinforcement due to the alkalinity of concrete [Mufti et al, 2005]. However, steel rebar used to reinforce concrete structures will commonly begin to corrode well within this time range.

Another important distinction exists between the degradation mechanisms of steel and GFRP reinforcement. The corrosion reaction associated with the degradation of steel rebar results in an increase in volume, which leads to increased cracking and spalling, allowing more access for moisture infiltration, and in turn, further degradation. Improvements to resins in recent years have dramatically improved the

resistance of GFRP materials to harsh environmental conditions. This will further improve the durability of GFRP materials in the concrete environment [Alsayed et al, 2002].

4. BOND BEHAVIOUR

4.1 Introduction

An important parameter to consider when investigating the long-term durability of a structural system is the bond performance and characteristics between material interfaces (i.e., reinforcement – epoxy interface, concrete – epoxy interface, reinforcement – concrete interface). The most common way of evaluating the bond performance of a particular structural component is by investigating the bond stress and slip behaviour – where slip can be defined as a relative displacement between an interface parallel to an applied force – at a particular interface. Most frequently, bond behaviour is examined at the interface between a reinforcing bar and the material in which the bar is embedded. Bond stress, u can be defined as the shear force per unit surface area of the interface. When calculating the bond stress on a reinforcing bar, the following equation can be used:

$$u = \frac{T}{\pi d_b I_d} \qquad \text{[Ehansi, 1996]}$$

where T = applied tensile force
d_b = rebar diameter
I_d = embedment length

The bond stress transfers the force applied to a reinforcing bar to the surrounding material (epoxy or concrete, etc).

The bond of reinforcement to concrete (and logically also to epoxy) is due to three main factors: chemical adhesion, friction, and mechanical bearing. The first represents the "gluing" of the two materials by the chemical properties of the cement paste (or epoxy), the second may be either static friction or sliding friction, and the third is a combination of the influence of surface roughness and deformation pattern, with the latter effect predominant. Deformed bars used in concrete generate the

majority of their bond strength from the mechanical bearing of the ribs against the surrounding concrete. For reinforcement that does not possess a significantly deformed surface, the load carrying capacity depends only on the adhesion between the bar and the grout prior to debonding, and on friction thereafter [Nilson, 1968; Benmokrane, 1996].

Other factors have been known to affect the bond strength between deformed bars and concrete such as the compressive strength of the surrounding concrete, the presence of confining stresses, the presence of splitting cracks, and (in the case of steel bars) the yielding of reinforcement [Lundgren, 2000; Rossetti, 1995].

4.2 Theoretical Bond – Slip Relationship [Nilson, 1968]

The theoretical relationship between bond stress and bond slip of an element of a reinforcing bar embedded in concrete is shown graphically in Figure 5. The slip displacement shown is the relative movement of the reinforcing bar to the reinforcing bar – concrete interface under an applied pullout load. Prior to overcoming the resistance of adhesion and static friction there will be virtually no displacement. This is shown graphically by the theoretical vertical line a-b, where no slip displacement has occurred under the applied pullout load.

Once the limit of adhesion and static friction is exceeded, the adhesion bond is destroyed and the load drops to the value c, which is governed by sliding friction. Upon further loading and further slippage, the mechanical bearing forces are engaged as the interlocking effect of the bar deformations become significant. At this stage the bond stress is the sum of the sliding friction and mechanical bearing of the bar, with the latter component being more dominant as the displacement increases.

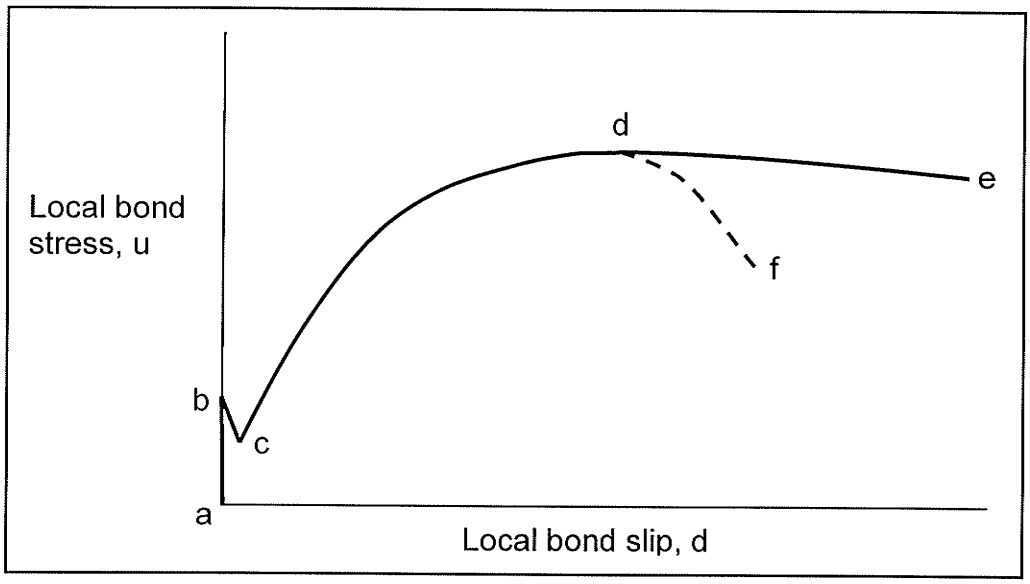

Figure 5. Theoretical Bond Stress – Bond Slip Relationship.

In the slip stage between c and d, relative displacement may occur between reinforcement and concrete at the interface, with slight crushing of the concrete ahead of the bar deformations; or displacements may be along a new cylindrical failure surface concentric with the reinforcing bar, some small distance out from the concrete – bar interface. In either case, a nonlinear relationship is expected, until a maximum bond stress is reached at d.

Performance beyond point d is governed by the depth of the bar within the concrete block. If the bar element is deep within the concrete, far from any end surface or crack face, then the local average bond stress will remain virtually constant, with a slight decrease experienced due to diminishing diameter resulting from Poisson's Effect. The portion of the curve d – e is the result.

However, if the bar element is near a crack face or near the edge of the concrete surface then longitudinal cracks may form along the reinforcing bar. Alternatively, the presence of high principal tensile stresses near the concrete face may lead to cone-shaped failure surfaces concentric with the bar. Either of these cases will

result in local bond stress falling nearly to zero and the element's terminal point will be point d. Furthermore, a bar element that is intermediate in terms of its depth in the concrete block, that is, if an element is neither sufficiently deep in a concrete block nor sufficiently near a cracked or free surface, then the element will produce a descending bond – slip curve falling from d to an arbitrary point f.

4.3 Bond Effects of GFRP Bars

Generally, the slip of GFRP bars under applied pullout load is larger than that observed with steel bars due to two main differences between GFRP and steel bars. First, the lower modulus of elasticity of GFRP allows greater elongation over the entire bond length. Second, for sand coated GFRP rebar, the adhesion and friction components control the bond strength. This is not the case with steel rebar where mechanical bearing is the major source of bond strength. These weaker components of bond strength cannot resist large bond stresses and may result in greater slip [Ehansi, 1996; Benmokrane, 1997].

A large amount of research has used the pullout test as both an indicator and a means of comparison of bond strength between various types of reinforcing bars and various external surface conditions of reinforcing bars [Kayyali, 1995]. The pullout test has been employed in this study to evaluate bond characteristics of different reinforcing bars and will be outlined later in this report.

5. EXPERIMENTAL PROGRAM

The experimental program was designed to identify which marker mounting assembly would have the best long-term structural performance when exposed to conditions that would most likely cause damage to these monuments over the course of their service life. The most common source of damage to monuments at Brookside Cemetery was the result of harsh environmental conditions (freeze/thaw cycles with moisture exposure), therefore, the long-term durability performance of the structural components was particularly important to evaluate.

To accomplish the durability evaluation of the marker mounting assemblies, methodologies were used to accelerate degradation (freeze/thaw cycles with moisture exposure and high humidity) prior to mechanical testing. The freeze thaw program used in this study was developed following the guidelines of ASTM C666 (1997) Standard Test Method for Resistance of Concrete to Rapid Freezing and Thawing, ASTM E1512 (1993) Standard Test Method for Testing Bond Performance of Adhesive-bonded Anchors, and ASTM E488 (1996) Standard Test Methods for Strength of Anchors in Concrete and Masonry Elements. Following the environmental conditioning, pullout and lateral tests were performed to evaluate the strength each marker mounting assembly.

The durability performance of the reinforced concrete support beam was also investigated. Prior to mechanical testing, support beam test specimens were placed in an environmental chamber and exposed to the same freeze/thaw cycles as the marker mounting assembly specimens. During the temperature cycling, the specimens were also subjected to shear and bending stresses which were intended to accelerate the effects of the conditioning. The combination of sustained load and extreme freeze/thaw cycling is intended to replicate the actual service conditions of the support beam specimens. Following this conditioning, bending and shear force

capacity tests were performed to evaluate the behaviour of the GFRP and steel reinforced concrete beams.

5.1 Test Variables

Four variables were considered in the experimental program: mounting method, reinforcement material used in the support beam, mounting pin material, and marker granite type - and have been listed in Table 1.

Table 1. Test variables considered in the experimental program.

Mounting Method	Support Beam Reinforcement	Mounting Pin Material	Marker Material
- Pinning - Pocket - Bumper	- GFRP Reinforcement - Steel Rebar	- GFRP Mounting Pins - Threaded Stainless Steel Mounting Pins	- Stanstead Granite - Barre Granite

5.2 Mounting Methods

The specimens used for laboratory investigation at the University of Manitoba are full scale cross-sections of the support beams used at Brookside Cemetery, but are only 1.22 m in length. The actual length of specimens at the cemetery is 7.32 m. The beams are 610 mm wide and 229 mm deep at center, tapering to 203 mm deep at the edges. The typical support beam cross section is shown in Figure 6.

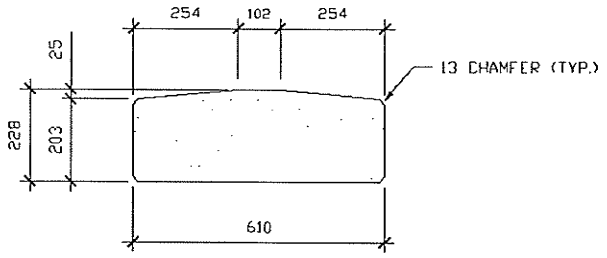

Figure 6. Support beam cross section.

Three marker mounting methods have been evaluated in this study. The first method, called the 'pinning method', involves attaching the granite marker to two mounting pins that have been anchored in 152 mm holes in the support beam with epoxy. Stainless steel and GFRP mounting pins that protruded 305 mm and 152 mm from the support beam have been investigated. All pins are 16 mm in diameter. The second method, called the 'pocket method', is similar to the method already used at Brookside Cemetery, except slots are formed during the casting of the beam, instead of cutting slots into the concrete after it has cured. The forming of the slot is intended to reduce stress concentrations and the onset of premature cracking. The third method, the Common Wealth War Grave Commission (CWGC) or 'bumper method" supports the marker by concrete 'bumpers' located on either side of the grave marker. The three marker mounting methods are shown graphically in Figure 7.

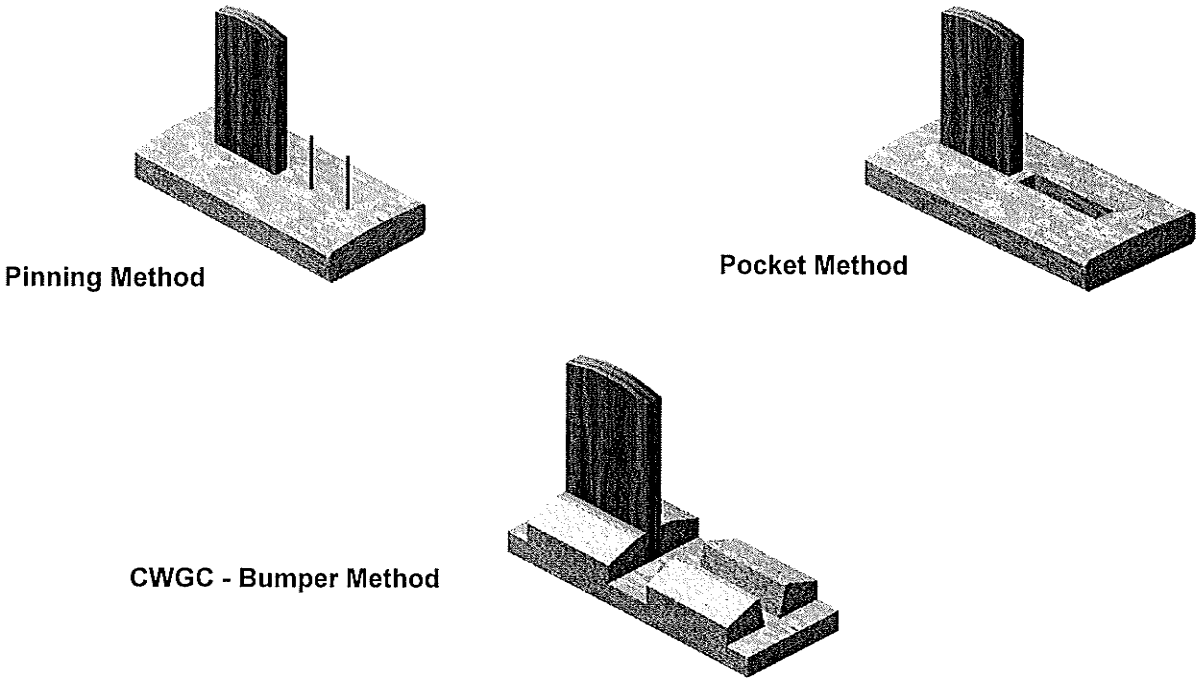

Figure 7. Marker mounting assemblies to be evaluated.

5.3 Test Materials

Cowin Steel Co. of Winnipeg, Manitoba provided the steel reinforcement and stainless steel rods. Both materials have a yield strength of 400 MPa.

The GFRP material investigated was V-ROD™ manufactured by ADS Group Composites Inc. Division Pultrall Quebec, Canada. The rods are made of continuous longitudinal "E-glass" fibre strands (60% by volume) bound together with a vinylester resin (40% by volume) using the pultrusion process. The rods are covered with a coating of sand particles of a specific size distribution to enhance surface bonding potential. The mechanical properties of the GFRP bars are listed in Table 2.

Table 2. Mechanical Properties of GFRP V-ROD™ Bars.

Mechanical Properties	Unit	Bar Designation		
		#3	#5	#6
Bar diameter	Inches	0.38	0.63	0.75
Tensile modulus of elasticity (E*f*)	Gpa	45	46	42
Ultimate tensile strength (*fu*)	MPa	796	794	666
Guaranteed design tensile strength (*ffu*)	MPa	778	803	612
Allowable tensile stress (*ffa*)	MPa	195	201	153
Development strength (*ldf*)	mm	200	320	400
Flexural strength (*ffl*)	MPa	1075	1190	977
Flexural modulus of elasticity (E*fl*)	Gpa	46	47	47
Ultimate strain in flexure (E*fl*)	%	2.4	2.5	2.1
Shear strength (Fs)	MPa	221	206	204
Longitudinal coefficient of thermal expansion (aL)	10^{-6}/ °C	7.7	11.3	8.5

The grave marker materials used in the study were Barre grey or Stanstead grey granite. The Barre grey granite was obtained from quarry division in Barre, Vermont USA. Graniteville, Quebec, Canada supplied the Stanstead grey granite.

5.4 Reinforced Concrete Support Beam Design

The reinforced concrete support beams used in this study were designed in accordance with the Concrete Design Handbook A23.3-94, and ISIS Canada Design Manual III (Rizkalla and Mufti, 2001).

The applied moment and shear forces were calculated based on a 7.32 m support beam, which is the length most commonly used at Brookside Cemetery. There were three loads assumed to act on the beam: 1) a uniformly distributed load due to the self weight of the beam (factored dead load = 3.12 kN/m), b) a uniformly distributed snow load (factored live load = 1.16 kN/m), and c) point loads due to the weight of the markers which were spaced every four feet (factored dead load = 0.833 kN per marker). This loading condition produced a maximum shear force of 23 kN at the supports, and a maximum bending moment of 42 kNm at mid-span. The loading conditions, shear force diagram, and bending moment diagram are shown in Figure 8.

The 1.22 m laboratory specimens were designed to resist the same load effects as the 7.32 m support beam – namely, the 1.22 m specimens were designed to resist a minimum moment of 42 kNm and a minimum shear force of 23 kN. As these specimens were designed to be tested in a controlled laboratory environment, the material strength reduction factors, which are normally used in design have all been set to unity. Furthermore, the value used for the compressive strength of concrete, f'_c, was assumed to be 35 MPa for design, however, subsequent compressive strength tests performed on concrete cylinders of the same concrete mix were found to have an average 28-day compressive strength of 54.2 MPa.

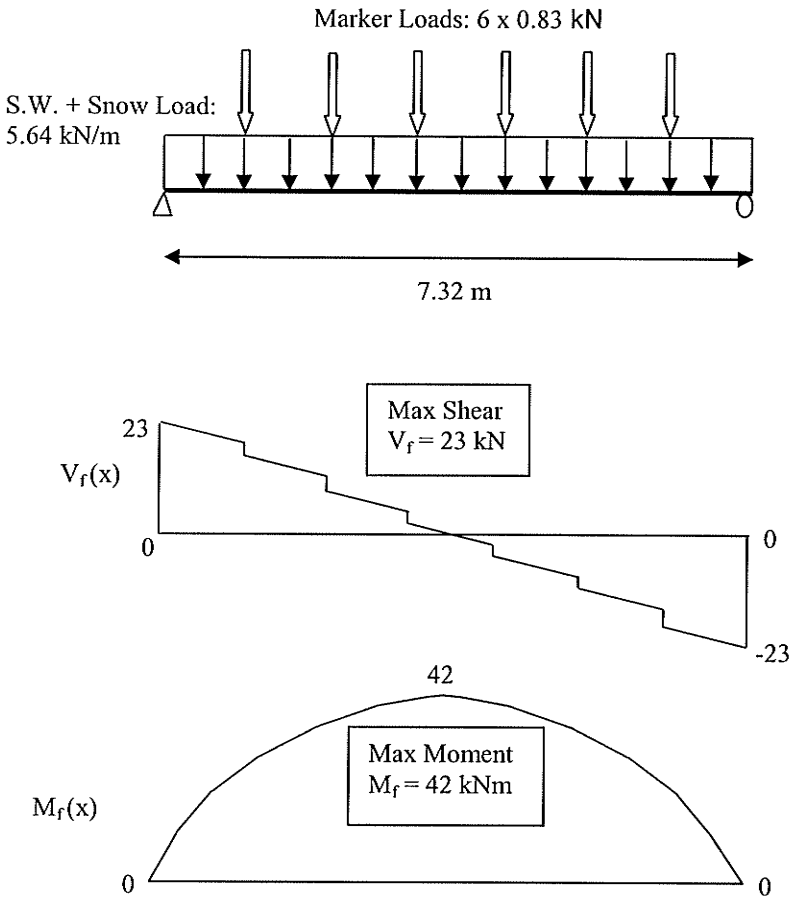

Figure 8. Shear and bending moment diagrams for 7.32 m beam.

Shear design, steel: The concrete beams reinforced with steel were found to have a shear resistance due to concrete, V_c, of 110 kN which is significantly higher than the applied factored shear of 23 kN. The following equation (Concrete Design Handbook A23.3-94) was used to calculate the shear resistance, V_c, of beams reinforced with steel.

$$V_c = 0.2\lambda\phi_c\sqrt{f'_c}\,b_w d$$

λ = Modification factor for density of concrete (1.0)
ϕ_c = Material resistance factor for concrete, 0.65 (set to 1.0 for lab design)
f'_c = Compressive strength of concrete (assumed 35 Mpa)

b_w = Width of beam (609.6 mm)

d = Distance from the extreme compression surface to the centroid of the reinforcement (152 mm)

$$V_c = 0.2 \times 1.0 \times \sqrt{35} \times 609.6 \times 152 \times 10^{-3} = 110 \text{ kN}$$

Since the shear resistance of concrete is higher than the factored shear, V_f, no additional shear reinforcement was required. However, in order to monitor the behaviour of the steel stirrups during testing, minimum shear reinforcement was specified. A 6M stirrup (which has a smaller cross sectional area than most commonly used stirrups) was the largest stirrup that could be bent around the tight radius of the relatively shallow beams (h = 229 mm). Since these smaller stirrups were used, a relatively small spacing of 100 mm was required to meet the minimum reinforcement criteria. The steel stirrups provided an additional 38 kN of shear resistance for a total of 148 kN of shear resistance. The following equations (Concrete Design Handbook A23.3-94) were used to calculate the additional shear resistance supplied by the steel stirrups, V_s, and the total shear resistance of the reinforced concrete beam, V_r.

$$V_s = \frac{\phi_s A_v F_y d}{s}$$

ϕ_c = Material resistance factor for steel, 0.85 (set to 1.0 for lab design)

A_v = Total cross sectional area of each leg of steel shear reinforcement (31.7 mm^2 x 2 legs)

F_y = Yield stress of steel reinforcement (400 MPa)

d = Distance from the extreme compression surface to the centroid of the reinforcement (152 mm)

s = Stirrup spacing (100 mm)

$$V_s = \left(\frac{1.0 \times (31.7 \times 2) \times 400 \times 152}{100}\right) \times 10^{-3} = 38.5 \text{ kN}$$

$$V_r = V_c + V_s$$

V_r = Total shear resistance of member

V_r = 110 kN + 38.5 kN = 148.5 kN

Shear design, GFRP: The shear resistance of concrete is lower for beams reinforced with GFRP than for beams reinforced with steel because of the difference in stiffness of the two reinforcement materials. Generally, GFRP reinforced beams are less stiff (will experience more deflection at the same load) than steel reinforced beams which means that after cracking, the neutral axis of GFRP reinforced beams is higher (the neutral axis shifts upward with increased deflection). Since the neutral axis is higher in GFRP reinforced beams, less of the section is in compression, and subjecting a concrete member to compression greatly improves its shear resistance. For this reason the shear resistance of concrete for the GFRP reinforced beam, Vc, was 53 kN (compared to a shear resistance of 110 kN for the beams reinforced with steel). The following equation (Rizkalla and Mufti, 2003) was used to calculate the shear resistance, V_c, of the concrete in the GFRP reinforced support beams.

$$V_c = 0.2\phi_c \sqrt{f'_c} b_w d \sqrt{\frac{E_{FRP}}{E_s}}$$

E_{FRP} = Young's Modulus of FRP stirrups (46 GPa)

E_s = Young's Modulus of Steel (200 GPa)

$$V_c = \left(0.2 \times 1.0 \sqrt{35} \times 609.6 \times 152 \sqrt{\frac{46}{200}}\right) \times 10^{-3} = 52.6 \text{ kN}$$

Again, the shear resistance of the concrete is greater than the applied factored shear of 23 kN, so no additional stirrups were required. However, in order to study the behaviour of the GFRP stirrups in the specimens, V-ROD™ #3 (0.38" diameter) stirrups were specified at a spacing of 100 mm. The same stirrup spacing was chosen for the GFRP and Steel reinforced beams to facilitate the comparison of stirrup strains during testing. The GFRP stirrups provided an additional 123 kN of shear resistance for a total of 176 kN of shear resistance. The following equations (Rizkalla and Mufti, 2003) were used to calculate the additional shear resistance supplied by the GFRP stirrups and the total shear resistance of the GFRP reinforced beam.

$$F_{FRPu} = F_{FRPg}\left(0.4 + 0.015\frac{l_{FRPd}}{d_e}\right)$$

F_{FRPu} = Ultimate tensile strength of stirrup

F_{FRPg} = Guaranteed tensile strength of FRP stirrup (778 MPa)

l_{FRPd} = Development length (200 mm)

d_e = Effective diameter, $\sqrt{\frac{4\times A_{bar}}{\pi}} = \sqrt{\frac{4\times 73.17}{3.14}} = 9.65$ mm

$$F_{FRPu} = 778\left(0.4 + 0.015\frac{200}{9.65}\right) = 553 \text{ MPa}$$

$$V_{FRP} = \frac{\phi_{FRP} A_{FRP} X F_{FRPu} d}{s} \le 0.8\lambda\phi_c\sqrt{f'_c}\, b_w d\sqrt{\frac{E_{FRP}}{E_s}}$$

θ_{FRP} = Material resistance factor of FRP (0.4 for GFRP, set to 1.0 for lab design)

A_{FRP} = Total cross sectional area of each leg of FRP shear reinforcement, (73.14 mm^2 x 2 legs)

X = Reduction factor used for design purposes, 0.4 (set to 1.0 for lab design)

$$V_{FRP} = \left(\frac{1.0(73.14 \times 2) \times 1.0 \times 553 \times 152}{100} \right) \times 10^{-3} = 123kN$$

$$\leq \left(0.8 \times 1.0 \times 1.0\sqrt{35} \times 609.6 \times 152 \sqrt{\frac{46}{200}} \right) \times 10^{-3} = 210kN$$

$\rightarrow V_{FRP}$ =123 kN

$$V_r = V_c + V_{FRP}$$

V_r = 52.6 + 123 kN = 176 kN

Flexural design, steel: The steel reinforced concrete beams contained 2-20M bars and 4-15M bars running longitudinally to resist bending moments, for a total area of steel of 1400 mm^2. The following equations to calculate moment resistance are based on the provisions of the Concrete Design Handbook A23.3-94. The steel reinforced support beams were found to have a theoretical moment resistance, M_r, of 76 kNm. This is higher than the factored applied moment of 42 kNm.

$$\rho_{\max} = \left(\frac{\alpha_1 \beta_1 \phi_c f'_c}{\phi_s f_y} \right) \left(\frac{700}{700 + f_y} \right)$$

$\rho_{\max}$ = Maximum reinforcement ratio that ensures a tension failure (this is a desirable failure for steel reinforced beams as it ensures large deflection prior to failure due to the yielding of steel reinforcement)

$\alpha_1 =$ Ratio of average stress in rectangular compression block to the specified concrete strength (0.80 for $f'_c =$ 35 MPa)

$\beta_1 =$ Ratio of depth of rectangular compression block to depth to the neutral axis (0.88 for $f'_c = 35$ MPa)

$$\rho_{max} = \left(\frac{0.8 \times 0.88 \times 1.0 \times 35}{1.0 \times 400}\right)\left(\frac{700}{700+400}\right) = 0.0392$$

$$\rho = \frac{A_s}{b \times d}$$

$\rho =$ Actual reinforcement ratio of steel reinforced section

$A_s =$ Area of longitudinal steel reinforcement provided (1400 mm^2)

$$\rho = \frac{1400}{609.6 \times 152} = 0.0151$$

→ Since $\rho \leq \rho_{max}$ tension failure will govern.

$$c = \frac{A_s \phi_s f_y}{\alpha_1 \beta_1 \phi_c f'_c b}$$

$c =$ Depth to neutral axis

$$c = \frac{1400 \times 1.0 \times 400}{0.80 \times 0.88 \times 1.0 \times 35 \times 609.6} = 37.3\,\text{mm}$$

$$M_r = T\left(d - \frac{\beta_1 c}{2}\right)$$

$M_r =$ Moment resistance of beam

$T =$ Tensile force at equilibrium, $= \phi_s A_s F_y = 1.0 \times 1400 \times 400 \times 10^{-3} = 560\,\text{kN}$

$$M_r = 560\left(152 - \frac{0.88 \times 37.3}{2}\right) \times 10^{-3} = 76.0\,\text{kNm}$$

Flexural design, GFRP: The GFRP reinforced beams were designed with 2-VR#6 (0.75" diameter) and 4-VR#5 (0.63" diameter) longitudinal GFRP bars to resist bending moments. The total area of GFRP was 1375 mm^2. Since the two bar sizes have different ultimate tensile strengths, a weighted average of the tensile strength value for each bar was taken and found to be 723 MPa. The following equations used to calculate the moment resistance of GFRP reinforced concrete beams are based on the provisions of the ISIS Canada Design Manual III. The GFRP reinforced support beams were found to have a moment resistance of 80 kNm which is higher than the factored applied moment of 42 kNm.

$$\rho_{FRPb} = \alpha_1 \beta_1 \frac{f'_c}{f_{FRPu}} \left(\frac{\varepsilon_{cu}}{\varepsilon_{cu} + \varepsilon_{FRPu}} \right)$$

$\rho_{FRPb} =$ The balanced reinforcement ratio; at this level of reinforcement a simultaneous tension and compression failure would occur (simultaneous failure of tension reinforcement and crushing of concrete)

$f_{FRPu} =$ Ultimate tensile strength of FRP reinforcing bars (723 MPa, weighted average)

$\varepsilon_{cu} =$ Ultimate design strain of concrete (0.0035)

$\varepsilon_{FRPu} =$ Ultimate strain of GFRP bars (0.0163, weighted average)

$$\rho_{FRP} = 0.79 \times 0.88 \times \frac{35}{723}\left(\frac{0.0035}{0.0035+0.0163}\right) = 0.0059$$

$$\rho = \frac{A_{FRP}}{b \times d}$$

ρ = Actual reinforcement ratio of FRP reinforced section

A_{FRP} = Cross sectional area of flexural FRP reinforcement provided (1375 mm^2)

$$\rho = \frac{1375}{609.6 \times 152} = 0.0148$$

Since $\rho > \rho_{FRPb}$, the section is over-reinforced and will fail by crushing of concrete (This is the most desirable failure mode for FRP reinforced beams because it provides more warning than a tension failure, which is very sudden because FRP does not yield like steel reinforcement).

$$f_{FRP} = 0.5 E_{FRP} \varepsilon_{cu}\left(\sqrt{1+\frac{4\alpha_1\beta_1 f'_c}{\rho_{FRP} E_{FRP} \varepsilon_{cu}}} - 1\right)$$

f_{FRP} = Amount of stress in FRP reinforcement in over-reinforced beams at equilibrium

E_{FRP} = Young's modulus of flexural FRP reinforcement (44,300 MPa, weighted average)

$$f_{FRP} = 0.5 \times 44{,}300 \times 0.0035\left(\sqrt{1+\frac{4 \times 0.79 \times 0.88 \times 35}{0.0148 \times 44{,}300 \times 0.0035}} - 1\right) = 433 \text{ MPa}$$

$$c = \frac{\phi_{FRP} A_{FRP} f_{FRP}}{\alpha_1 \beta_1 \phi_c f'_c b}$$

$$c = \frac{1.0 \times 1375 \times 433}{0.79 \times 0.88 \times 1.0 \times 35 \times 609.6} = 40.17 \text{ mm}$$

$$M_r = T\left(d - \frac{\beta_1 c}{2}\right)$$

T = Tensile force in FRP at equilibrium,

$$T = \phi_{FRP} A_{FRP} f_{FRP} = 1.0 \times 1375 \times 433.3 = 596 \text{ kN}$$

$$M_r = 596\left(152 - \frac{0.88 \times 40.17}{2}\right) \times 10^{-3} = 80 \text{ kNm}$$

5.5 Reinforced Concrete Beam Specimen Preparation

Forty-one 1.22 m reinforced concrete beam specimens were cast at Lafarge Canada inc. for the experimental program. The beams were cast in batches of seven beams, and tested for slump, air content and compressive strength at 1, 7, 14 and 28 days. The results for each of the six batches of concrete are shown in Table 3. In addition, six 1.22 m reinforced concrete beam specimens were salvaged from an unused 7.31 m precast steel reinforced concrete beam existing at Brookside Cemetery. These beam specimens were cast with an ordinary concrete mix and will be used as additional pullout test specimens, which will be referred to as 'old mix' specimens.

Table 3. Concrete properties for each concrete batch used in casting test specimens.

Concrete batch #	Air content (%)	Slump (mm)	Compressive strength (MPa)			
			1 day	7 days	14 days	28 days
1	4.2	120	25.5	44.5	48.3	57.6
2	4.8	110	32.1	45.0	46.9	58.2
3	5.6	150	24.1	41.7	44.7	46.0
4	5.4	120	18.9	28.0	33.5	35.7
5	5.0	120	31.0	32.1	39.8	48.3
6	4.4	130	18.1	49.4	50.8	58.7

5.5.1 Pullout specimen preparation

Twenty-six stainless steel rods and thirty GFRP rods were installed in fourteen 1.22 m beam specimens (4 rods per beam). All rods were 914 mm long and 16 mm in diameter. The rods were embedded in 152 mm deep holes that were 25.4 mm in diameter drilled in the center of the support beam specimens. The holes were filled with Hilti RE 500 epoxy adhesive. A schematic of the mounting rod embedment is shown in Figure 9. To improve bond characteristics, the stainless steel rods used in the study were threaded and the surface of the GFRP rods were covered in a coating of silica sand particles.

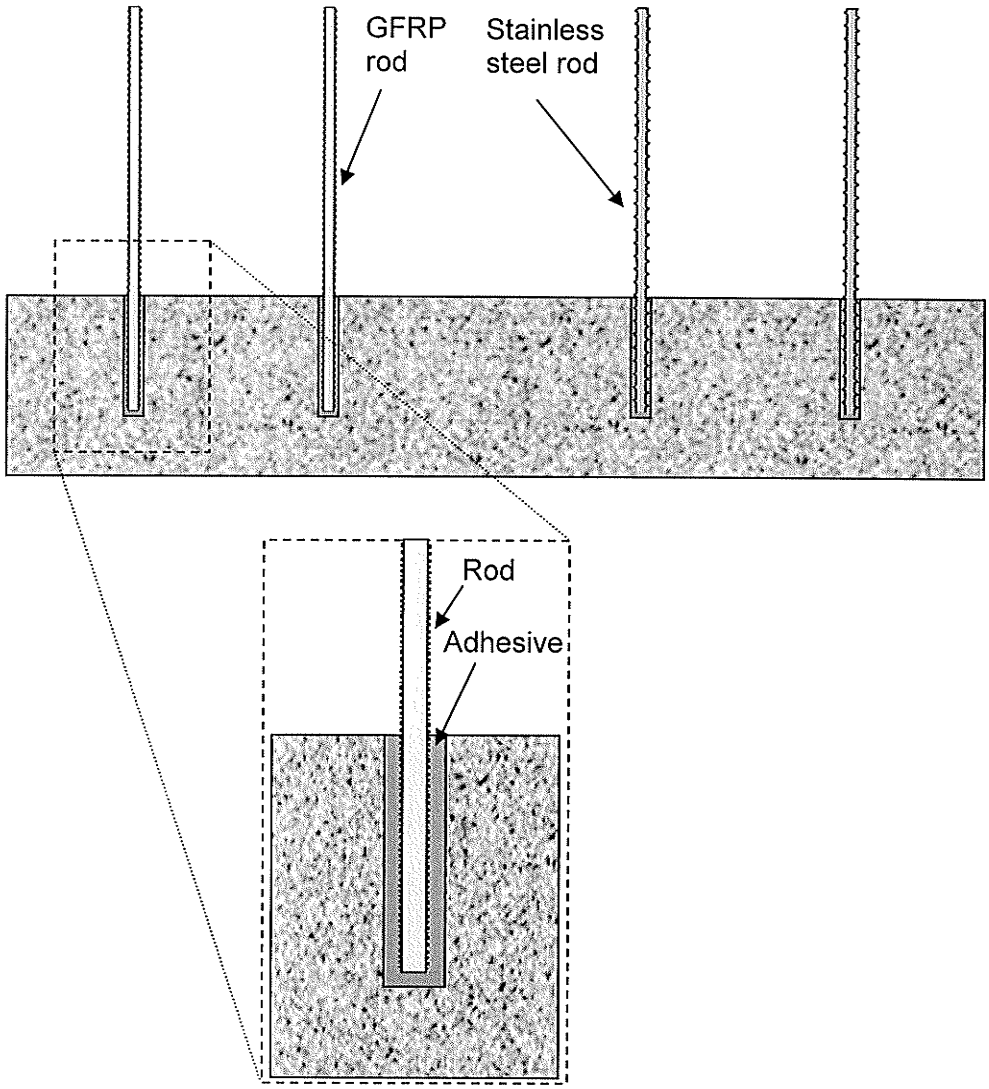

Figure 9. Schematic of marker mounting pins embedded in epoxy.

All mounting pins were embedded 152 mm in epoxy. Pultrall, the manufacturer of the #5 V-ROD ™ GFRP bars used in the study, specifies a 230 mm development length in concrete to develop the entire strength of the bar. Similarly, the CPCA Concrete Design Handbook (1998) specifies 323 mm as the development length of deformed steel bars (15.9 mm diameter) in concrete. This value, however, is for standard deformed steel rebar and the threaded stainless steel rods used in this study will have significantly better bond characteristics, and thus significantly shorter development length than typical deformed bars. Furthermore, the values of

development length for GFRP and steel bars were for embedment in concrete, not epoxy. Therefore, these values can only be used as rough approximations of what the actual development length will be for these materials in epoxy.

The embedment length will govern which failure mode is expected during testing. If bars are embedded at, or beyond their development length then rupture of the bar is expected. However, if the bars are embedded less than their development length, then a pullout type failure (a slip at the bar/epoxy interface) is expected.

5.5.2 Lateral test specimen preparation

The lateral test specimens were prepared using three marker mounting methods: pinning, pocket, and bumper. A total of twenty-two 1.22 m support beam specimens were mounted with 2 grave markers each yielding a total of 44 lateral tests. The types of lateral test specimens and variables are listed in table 4.

Table 4. Lateral test specimens.

Mounting method	Rod type	Adhesive type	Marker granite type	No. of specimens
Pinning	Steel	Hilti RE 500 Epoxy	Stanstead grey	7
			Barre grey	2
	GFRP	Hilti RE 500 Epoxy	Stanstead grey	7
			Barre grey	4
Pocket	-	Sika 212 grout	Stanstead grey	8
			Barre grey	4
CWGC-bumper	-	Sika 212 grout	Stanstead grey	8
			Barre grey	4

For the pinned specimens, the GFRP or stainless steel mounting pins were embedded in 152 mm of epoxy in the same manner as the pullout specimens (section 5.5.1). The grave markers were attached by drilling holes into the granite marker, filling them with epoxy, and sliding them over the protruding mounting pins. Two lengths of mounting pins were used in the study: 305 mm rods and 152 mm rods. A schematic of a pinned specimen is shown in Figure 10.

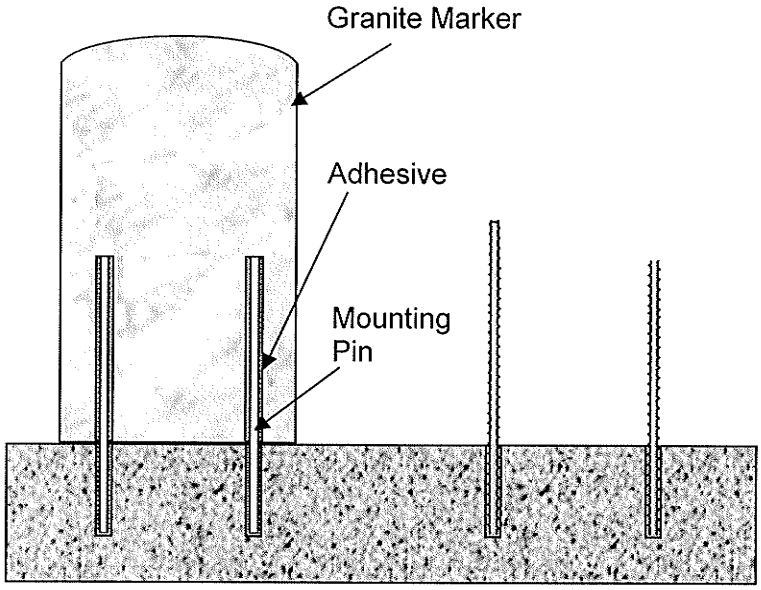

Figure 10. Schematic of pinned lateral test specimen preparation.

The pocket method specimens were made by placing a granite marker inside a slot that was formed during the casting of the support beams. Once the granite marker is lowered into the slot and leveled it is fixed in place by filling the void space with a slurry of Sika 212 grout. Similarly, the bumper method specimens were made by placing the granite marker between the concrete 'bumpers' and fixing them with grout. Figure 11 shows support beams for pinning, pocket and bumper specimens before the granite markers have been fixed in place.

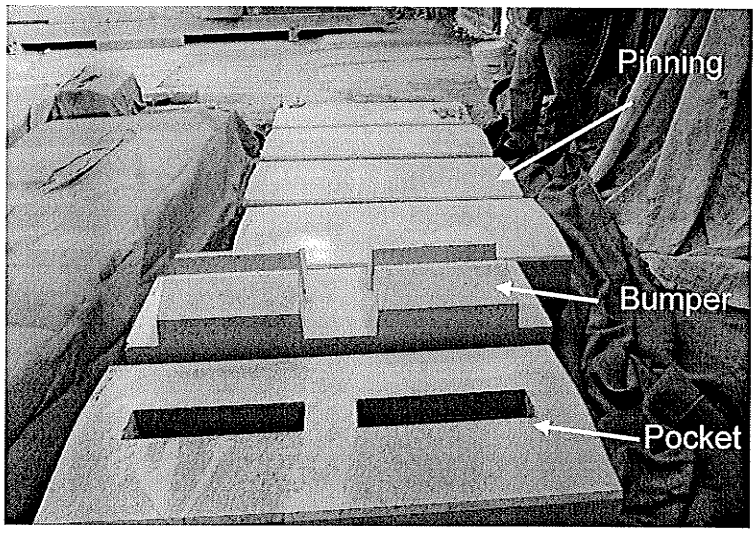

Figure 11. Lateral test specimens prior to attaching granite markers.

5.5.3 Shear and bending test specimen preparation

All of the support beam specimens used in the shear and bending evaluation are the same support beam cross-section as those used for the pinning method, that is, no pocket or bumper method specimens have been used for the shear or bending tests. The concrete cross-section and reinforcement scheme (GFRP or steel rebar) used in these bending test are the same as described in section 5.4.

5.6 Exposure Conditions

Prior to mechanical testing, the beams were subjected to a series of 50 freeze and thaw cycles in accordance with ASTM E 1512 (1993) – Standard Test Method for Testing Bond Performance of Adhesive-Bonded Anchors. This standard requires the temperature of the anchor and adhesive to cycle between -23° C and +40° C at 80% relative humidity and the area surrounding the adhesive and anchor to be covered with at least 12 mm of water. The temperature ranges dictated by this standard are also quite appropriate for the conditioning of the specimens to be used at Brookside Cemetery, as this range closely reflects the extreme temperatures that

these specimens would experience in the field under regular service conditions. To determine the effects of prolonged exposure to freeze/thaw conditions, one support beam test specimen, to be used for pullout testing with 2 stainless steel rods and 2 GFRP rods, was subjected to 250 cycles. Figure 12 shows pullout specimens inside the environmental chamber. Of the 47 beams used in this study, 35 were subjected to the freeze and thaw program and 12 were used as control specimens.

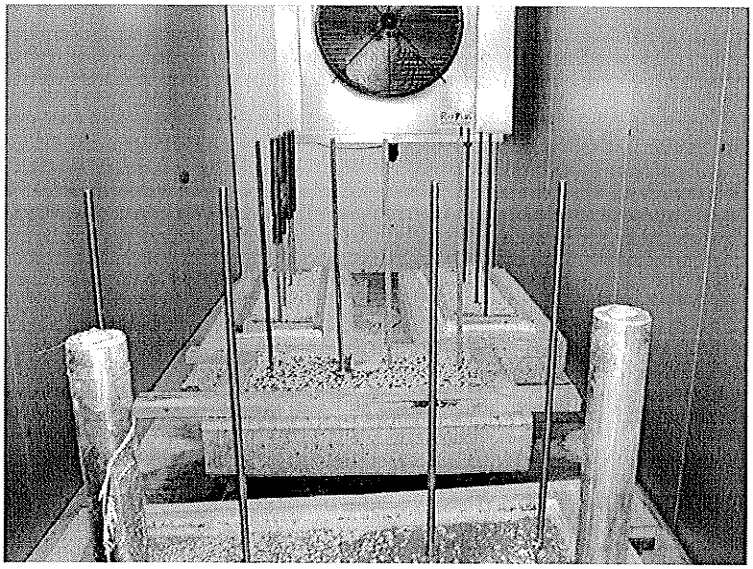

Figure 12. Pullout specimens in environmental chamber.

5.6.1 Temperature cycle profiles

Due to the large thermal mass of the specimens, there was a significant temperature lag between the core temperature of the test specimens and the ambient air temperature in the environmental chamber. In order to monitor the exact internal temperature of the specimens a thermocouple was placed and sealed inside a 152 mm hole drilled into one of the beams. The temperature cycle took approximately 22 hours to reach the desired temperature in the core of the specimens. Figure 13 shows a typical plot of the ambient air and beam core temperatures during conditioning.

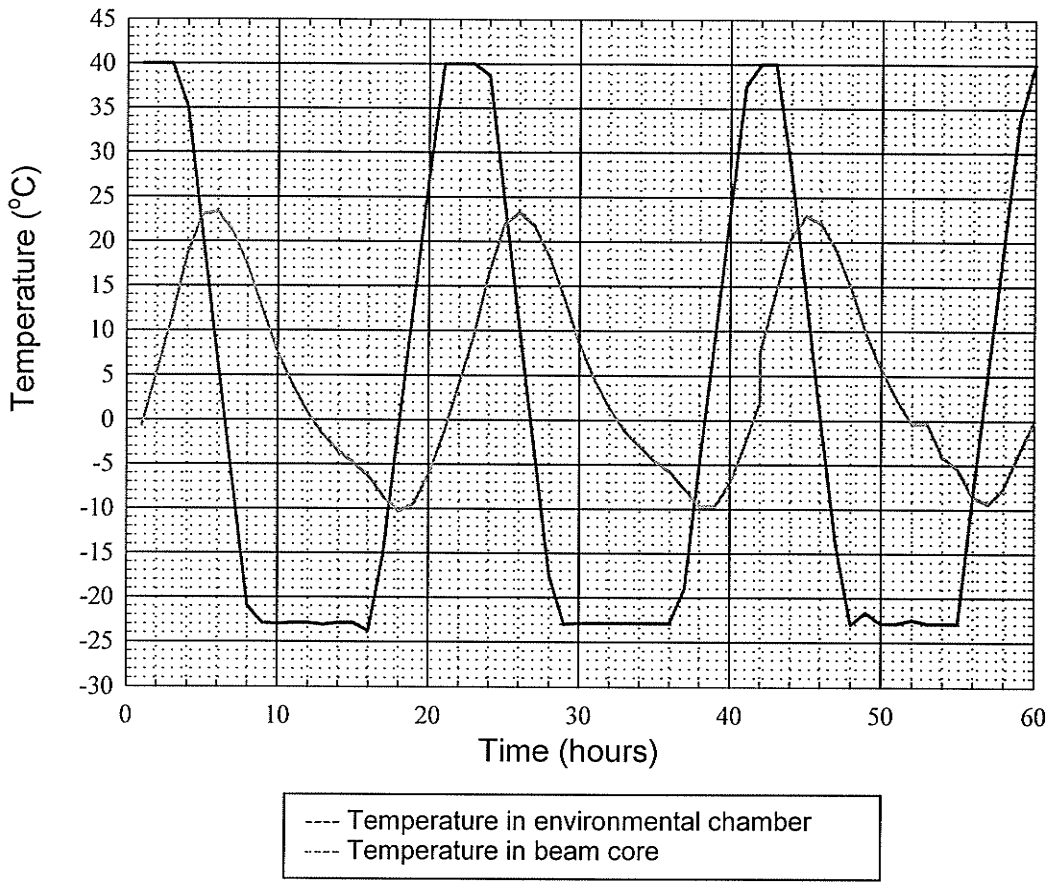

Figure 13. Freeze and thaw profile for test specimens.

The temperature in the core of the beam varies between extremes of about -10 °C and +23 °C per cycle. This range was considered to be sufficient to induce adequate freezing and thawing of all trapped moisture and water vapor throughout the section. In order for the core temperatures to experience an even wider range of extreme temperatures, the temperature cycles would require much longer than 24 hours, which was not feasible due to time constraints.

5.6.2 Specimen saturation

Frost action occurs when the moisture in concrete freezes and expands exerting pressure on surrounding concrete. If this pressure is large enough small cracks will form in the concrete, which are then easily infiltrated with additional available moisture. During a subsequent freezing cycle this moisture will freeze and expand, apply additional pressure, and create wider cracks allowing access to more moisture - and the cycle of damage continues. This type of frost action damage is responsible for much of the deterioration of concrete structures in Northern climates.

Conversely, dry materials that do not contain significant moisture do not suffer frost action damage; the degree of degradation that concrete members sustain under freeze/thaw conditions depends almost exclusively on the amount of available moisture. Therefore, prior to exposure to freeze/thaw cycles the test specimens were saturated in order to ensure that the freeze/thaw conditioning had the potential to cause frost action degradation.

Beam specimens were immersed in a saturated solution of Ca $(OH)_2$ for 72 hours prior to exposure to freeze/thaw cycles. A calcium hydroxide solution was chosen to saturate the beams because Ca $(OH)_2$ is a chemical compound closely related to the degradation mechanisms of concrete. Ca $(OH)_2$ is one of the compounds involved in the leaching and dissolution of concrete which dissolves hardened cement paste, increasing the concrete porosity (which improves moisture infiltration) and decreasing concrete strength. More information on the chemical reactions involved in the degradation of concrete can be found in the first technical report submitted for this project [Mufti et al, 2004]. Figure 14 shows several beam specimens immersed in the Calcium Hydroxide bath.

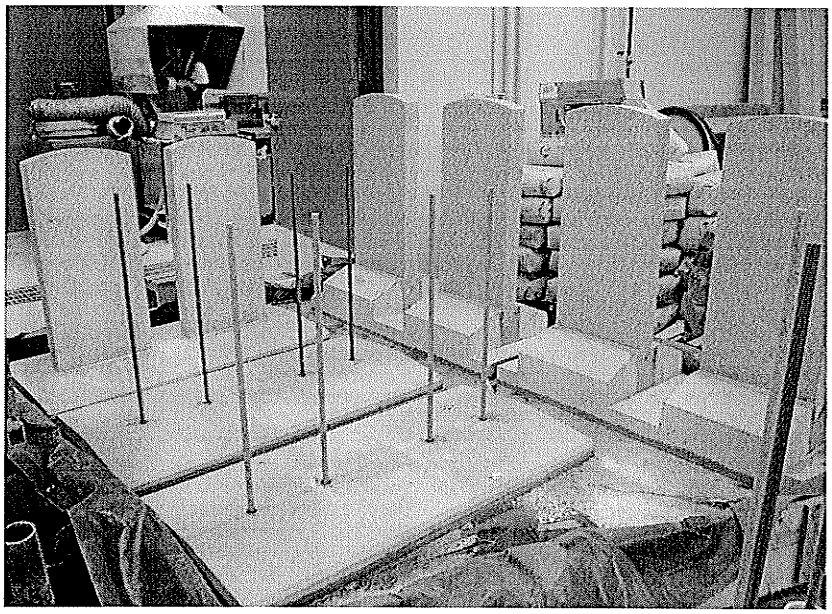

Figure 14. Specimens immersed in Ca $(OH)_2$ bath.

5.6.3 Sustained stresses on support beam specimens

As discussed in section 3.2, specimens reinforced with GFRP are often stressed while subjected to harsh environmental conditions to further accelerate their aging. Hence, the support beam specimens that were to be tested in bending and shear were both subjected to sustained loading while exposed to the freeze/thaw cycling program. Self reacting apparatus were designed to apply loads to the specimens while eliminating the need to have large reactions supported on the relatively weak floor of the environmental chamber. Using a self reacting apparatus also facilitates the conditioning of two specimens simultaneously.

Both of the apparatus used transferred the applied load through large coil springs. This was intended to reduce the effects of expansion and contraction during temperature cycling to ensure that the applied loading was virtually constant regardless of temperature fluctuation.

The Canadian Highway Bridge Design Code (CHBDC) published in 2000 specifies that the maximum sustained load applied to GFRP reinforcement cannot correspond to greater than 20% of the ultimate strain in the bar. This value is currently in consideration for being increased to 25% of ultimate strain for a future release of the standard. This experimental program intended to stress the bending and shear support beam specimens such that the GFRP reinforcement experienced 30% of ultimate strain, in order to determine if such a level of sustained stress is feasible.

5.6.3.1 Support beam specimens tested in bending

Since the support beam specimens are relatively short in length, the apparatus for applying sustained bending stresses in the environmental chamber incorporated a cantilever extension attached to the end of the specimens in order to increase the lever arm. This allowed larger bending stresses to be achieved with smaller loads, and also reduced the amount of shear stress exerted on the beams, which were intended to be subjected to pure bending. Figures 15 – 18 show photographs and schematics of the system.

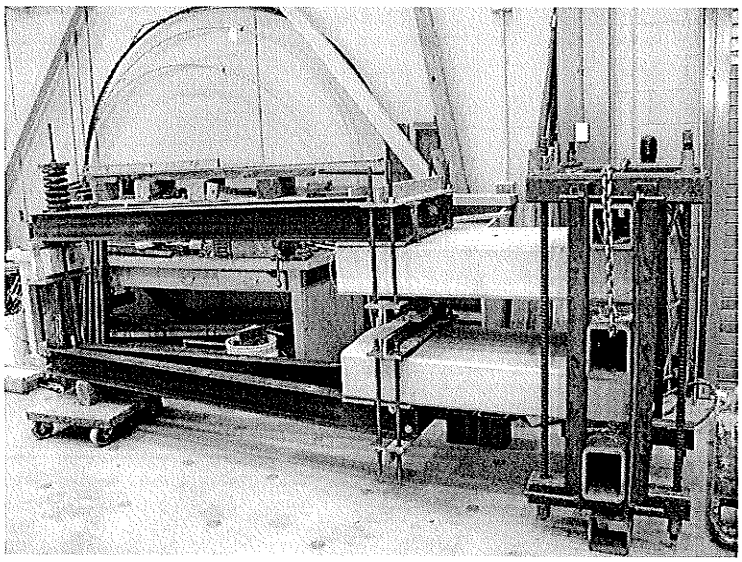

Figure 15. Self reacting sustained bending stress apparatus outside environmental chamber.

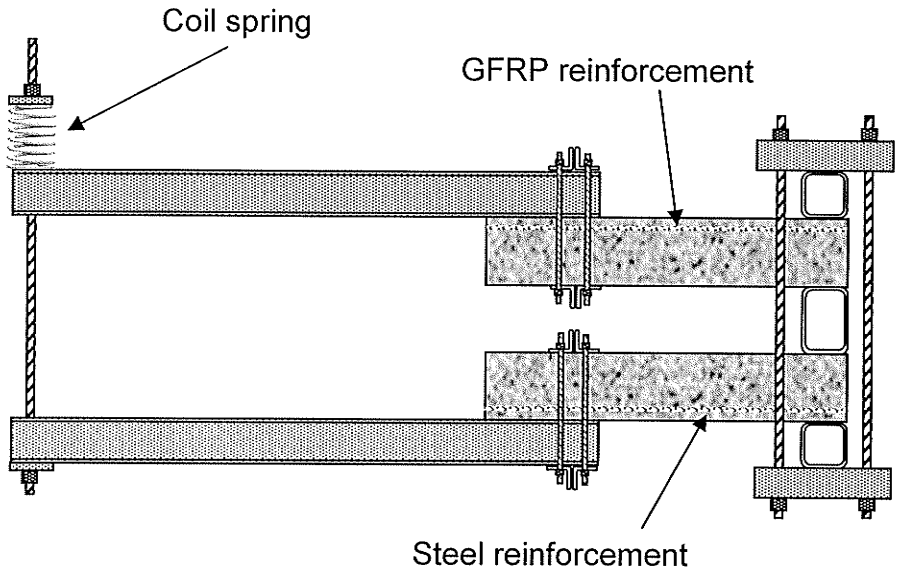

Figure 16. Schematic of bending stress apparatus.

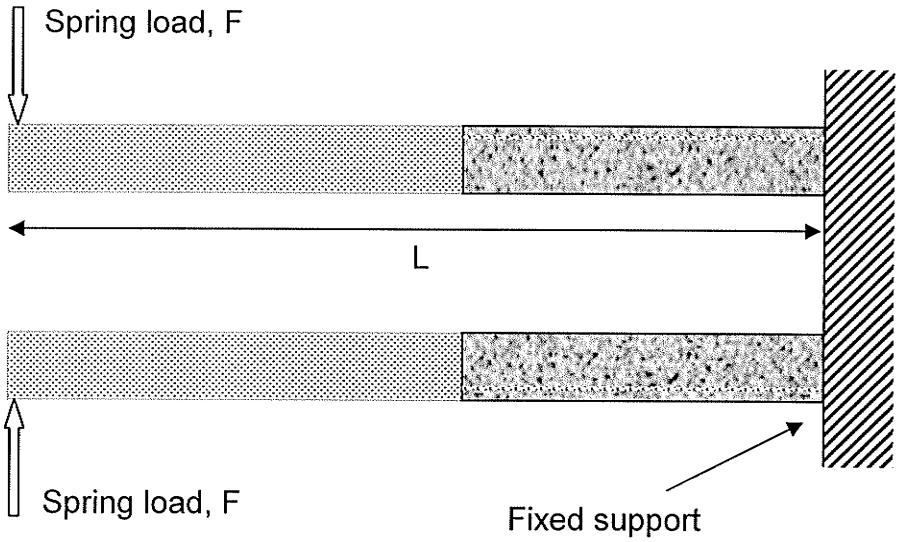

Figure 17. Bending apparatus equivalent to cantilever support.

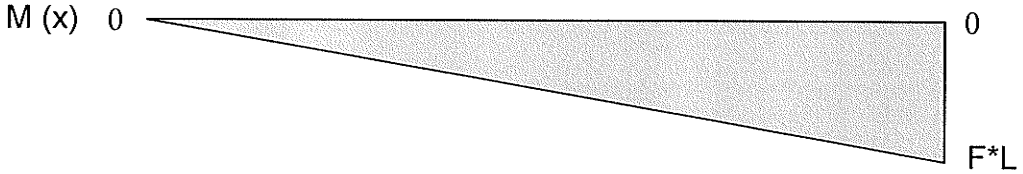

Figure 18. Bending moment diagram for bending specimens.

The strain in the longitudinal reinforcement was monitored by strain gauges that were attached to the reinforcing bars prior to casting. The tension in the spring supported bar was increased by tightening the nut, which in turn increased the bending stress on the specimens. The intended strain in the GFRP longitudinal reinforcing bar was 30% of the ultimate strain in tension: 30% x 0.016 = 0.0048 or 4800 microstrain. However, as the strain increased above 4000 microstrain, the GFRP reinforced specimen failed near the support.

It was later determined that the force couple acting at the fixed end of the beam to resist the applied moment created compressive forces that exceeded the compressive strength of the concrete. This lead to crushing of the concrete over the support as shown in Figure 19. Following this failure, it was decided to reduce the stress in the GFRP bars to 2000 microstrain during freeze/thaw cycling to avoid a similar compressive failure from reoccurring.

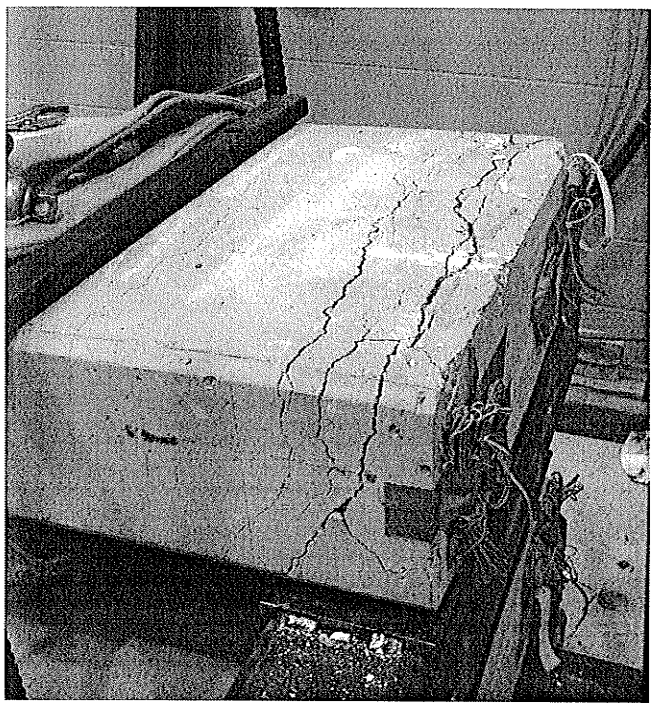

Figure 19. Compressive failure of concrete due to force couple over support.

5.6.3.2 Support beams tested in shear

The apparatus for applying sustained shear stress on support beam specimens during freeze/thaw cycling is detailed in Figures 20 - 23. Again, springs were used to alleviate the expansion and contraction effects in the tension bars under changing temperatures.

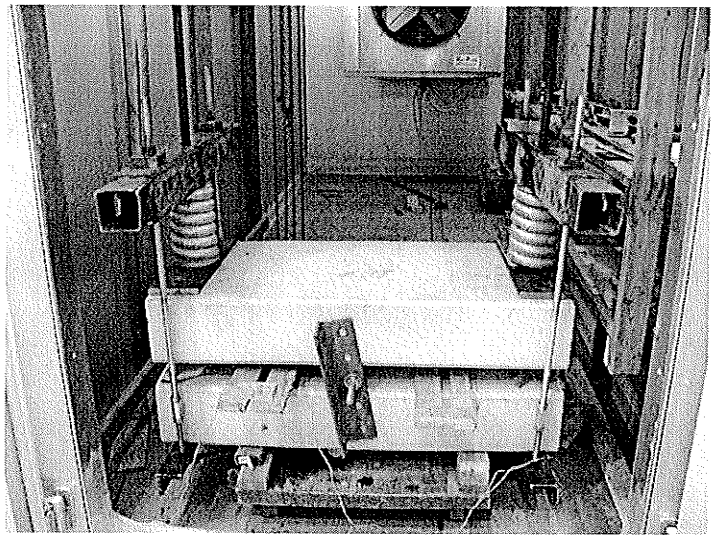

Figure 20. Sustained shear stress apparatus inside environmental chamber.

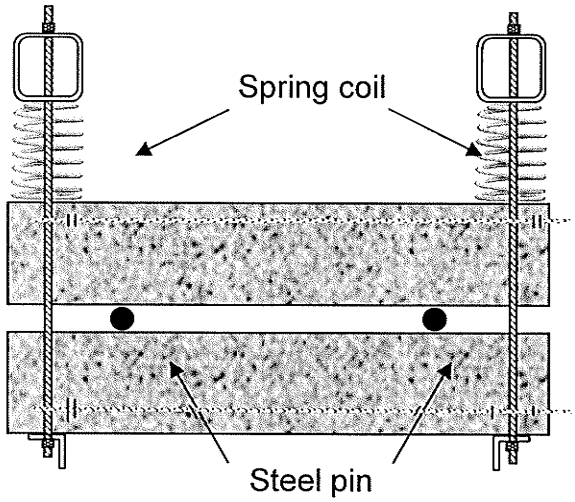

Figure 21. Schematic of sustained shear stress apparatus.

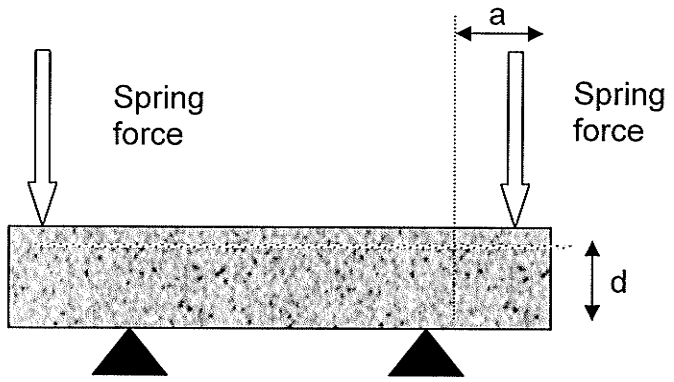

Figure 22. Shear stress apparatus equivalent to four point loading setup.

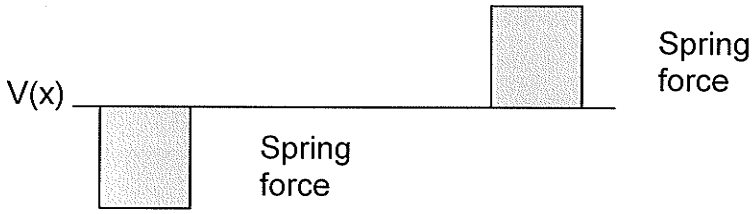

Figure 23. Shear stress diagram for shear test specimens.

Strains were monitored by strain gauges that had been attached to shear reinforcement (stirrups) at various distances along the beam prior to casting. Again, the desired sustained strain was 30% of the ultimate strain in the GFRP reinforcement during cycling, but there were difficulties achieving this level of strain before a bending failure would develop.

The governing factor in determining whether to expect a shear or flexural failure when loading a beam is the ratio of *a*, the distance from the applied load to the support, to *d*, the depth of the longitudinal reinforcement. Generally, beams with an *a/d* ratio less than one are referred to as 'deep beams' where shear stresses dominate. Flexural stresses are negligible and a truss or strut and tie model is utilized for analysis. In relatively short beams with *a/d* between 1 and 2.5, inclined cracks known as flexural-shear cracks initiate failure, but the actual failure will take place by either a shear-compression failure, or a shear-tension failure occurring

before the flexural strength of the section is attained. 'Normal' beams with *a/d* ratios between 2.5 and 6 may fail in either shear or flexure (depending on tension reinforcement, yield strength and concrete strength) and beyond an *a/d* ratio of 6, flexural failures govern [Pillai, 1999].

For the sustained shear stress setup, an *a/d* ratio of approximately 1.6 was chosen. This was to try to ensure that the beams would be governed by a shear failure while not being considered a 'deep beam', which involves more complex analysis. However, upon loading the system, severe vertical flexural cracks formed without any cracking appearing in the shear zone of the specimen. Approximately 100 kN of shear force (nearly four times the factored design shear load) was applied to the section which only produced a maximum strain in the GFRP shear reinforcement of approximately 400 microstrain. The specimens were subjected to freeze/thaw cycling without increasing the stress beyond this level for fear that increasing the load further would initiate a flexural failure. Figure 24 shows the propagation of flexural cracks in the loaded sustained shear stress specimen.

This unexpected behaviour may be attributed to the atypical geometry of the beam specimens. The support beam specimens are almost three times wider than they are deep; for typical reinforced concrete beams the opposite is true. Having such a shallow beam relative to its width makes beams especially weak in bending, and thus relatively strong in shear.

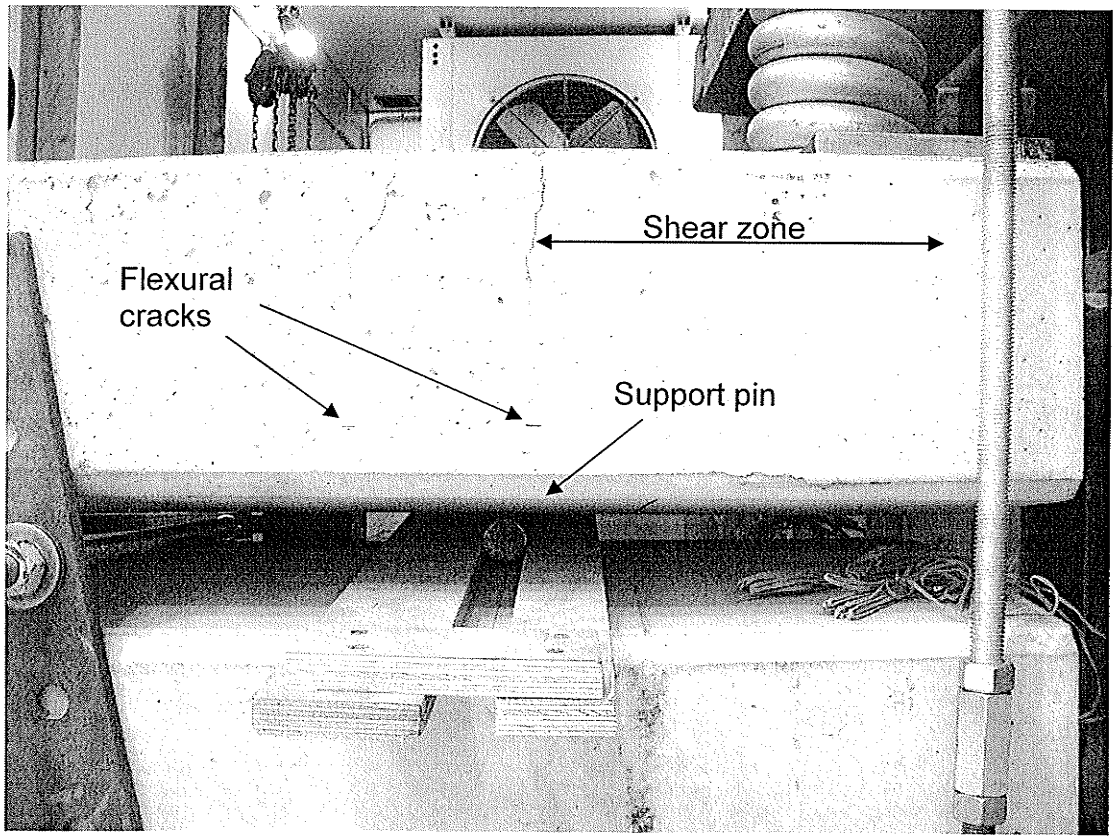

Figure 24. Flexural cracks almost propagate through entire section with no cracking in shear zone; *a/d* = 1.6.

5.7 Mechanical Tests

5.7.1 Pullout test

The purpose of the pullout tests was to evaluate the strength and durability of the bond between the marker mounting pin and the epoxy, and the bond between the epoxy and concrete, after exposure to the environmental conditioning program. A 1000 kN capacity MTS machine was used with a specially designed griping device to perform mounting pin pullout tests as shown in Figure 25.

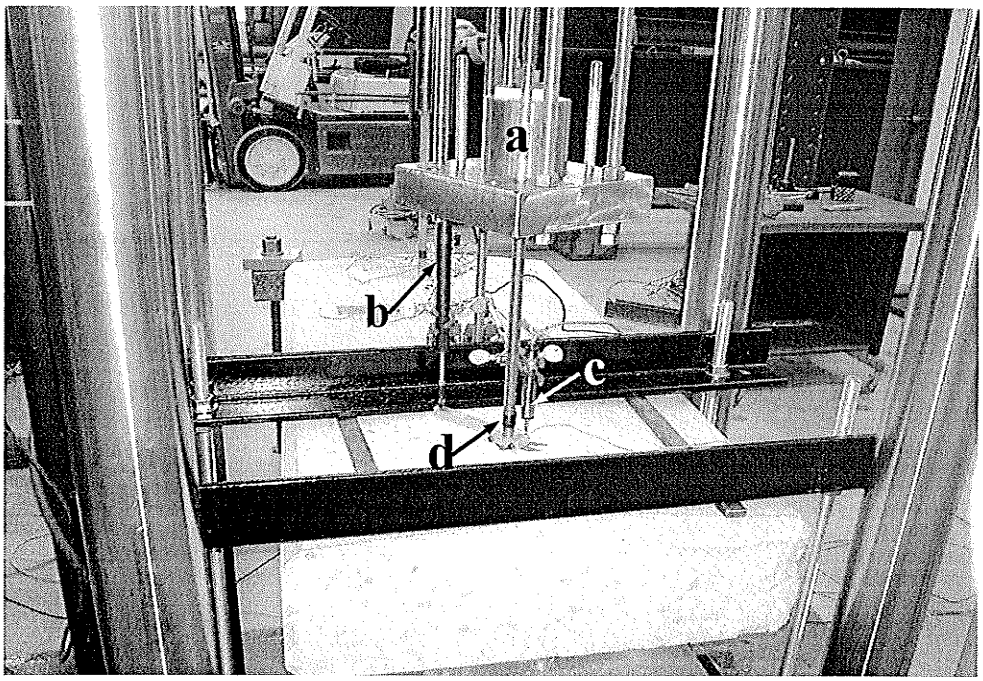

Figure 25. Laboratory setup for the pullout test: a) rod gripping system, b) and c) LVDTs at two locations, d) strain gauge.

Instrumentation included a linear variable differential transducer (LVDT) for measuring concrete deflection around the mounting pin relative to the support beam, an LVDT for measuring the slip of the mounting pin relative to the support beam, and a strain gauge attached to the mounting pin to measure strains during testing.

In order to prevent a crushing failure of the GFRP mounting pins during pullout testing, steel sleeves were placed over GFRP rods and were fixed with a highly expansive grout. The pullout test gripping system attached to threads that were cut in the steel sleeves, which prevented direct contact with the GFRP bars. The GFRP sleeves are shown in Figure 26. The stainless steel rods were already threaded which greatly facilitated attachment to the gripping system.

Figure 26. Steel sleeves fixed to GFRP rods to prevent crushing during pullout testing.

The pullout tests were performed monotonically at a rate of 1.5 mm/sec for the GFRP specimens and 4 mm/sec for the stainless steel specimens. The stainless steel specimens undergo significant elongation during yielding prior to failure; consequently the loading rate chosen for these specimens was increased to expedite test times.

5.7.2 Lateral test

The purpose of the lateral test was to evaluate the overall strength and durability of each of the marker mounting methods after environmental conditioning. The lateral tests were performed on full size granite markers using a servo controlled hydraulic actuator mounted horizontally to a rigid frame with the beam specimen secured to a strong floor, as shown in Figure 27. LVDTs were placed near the top, middle, and bottom of each granite marker to measure deflection along the length of the marker. Strain gauges were placed on each face of the marker to measure the compressive and tensile stress on the granite surface. During testing, the load was applied in 1 kN increments until failure.

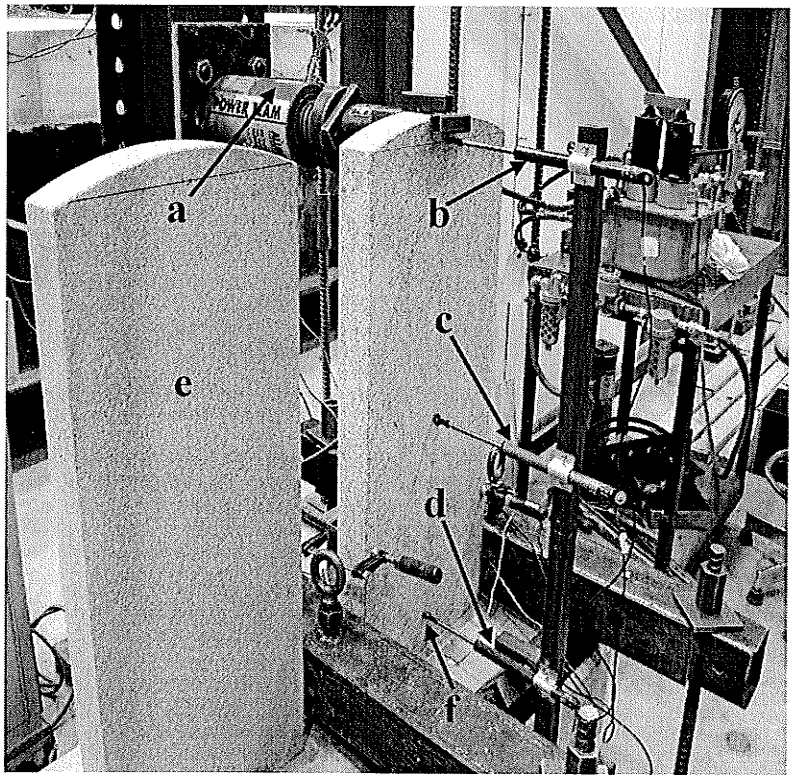

Figure 27. Laboratory lateral load test setup. A) horizontal load cell, b), c) and d) LVDTs at three locations, e) granite marker, f) strain gauge.

5.7.3 Shear test

The purpose of the shear test was to evaluate the shear performance of the new GFRP reinforced support beam design and compare it to steel reinforced specimens, and to evaluate the shear performance of specimens after combined exposure to sustained stresses and freeze/thaw cycles. The beam specimens were simply supported on 305 mm pin supports and loaded 266 mm from the centre of one end support to enable an a/d ratio of 1.75 during loading. The specimens were loaded with a 1000 kN MTS testing machine at a rate of 1 mm/min. The test setup is shown in Figure 28.

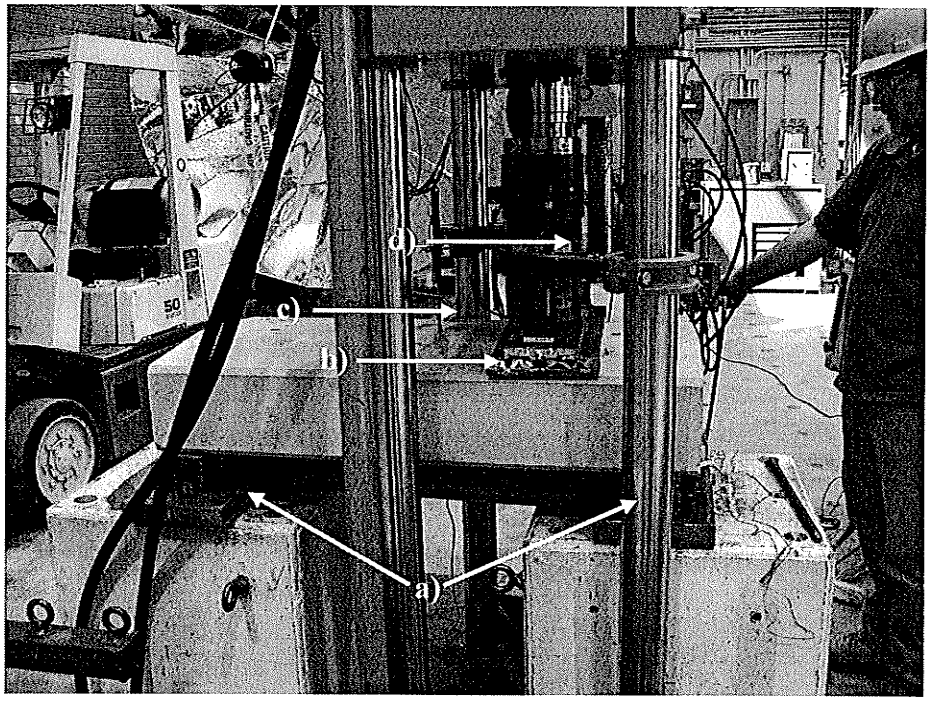

Figure 28. Shear test setup. a) pinned supports, b) contoured plate to evenly distribute load over specimen, c) LVDT to measure midspan deflection, d) LVDT to measure maximum deflection at the load application point.

The shear test specimens were instrumented with six strain gauges mounted on internal reinforcement prior to casting. Two gauges were attached to the longitudinal reinforcement at midspan to measure bending induced strains. Four gauges were mounted on the vertical legs of the stirrups: two gauges were mounted on the second stirrup located approximately 150 mm from the end of the beam, and two gauges were placed on the third stirrup located approximately 250 mm from the end of the beam. In addition, LVDTs were used to record deflections at midspan and at the point of the load application (the location of maximum deflection).

5.7.4 Bending test

The purpose of the bending test was to evaluate the performance of the new GFRP reinforced support beams and compare them to steel reinforced specimens, and to evaluate the effects of combined bending stress and exposure to freeze/thaw cycles.

A cantilever setup was originally designed to perform the bending tests and is shown in Figure 29.

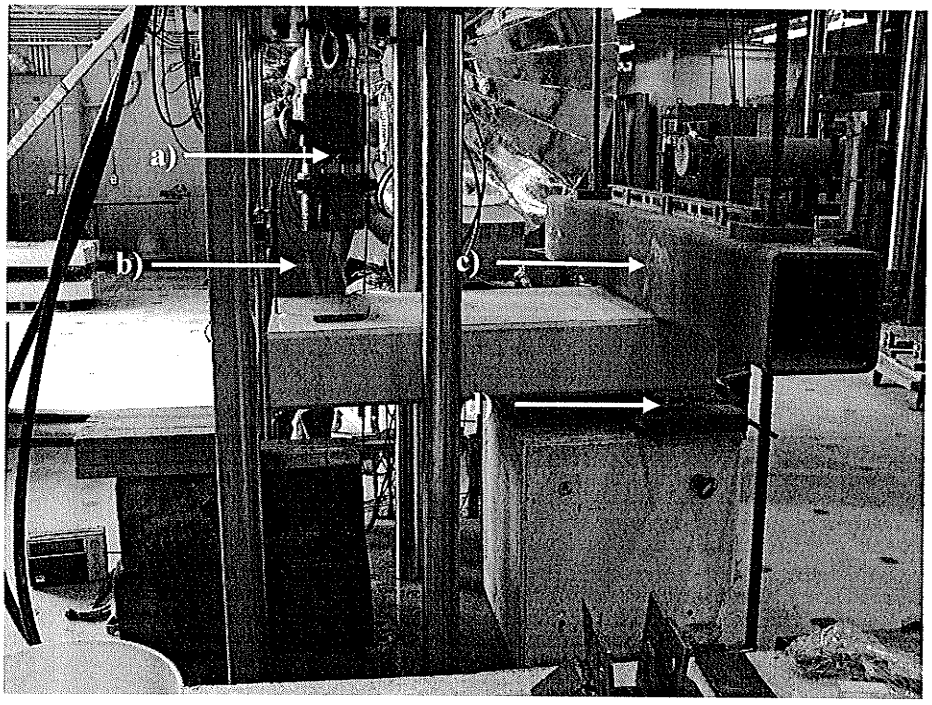

Figure 29. Cantilever bending test setup. a) actuator, b) LVDT for measuring tip deflection, c) HSS section stressed to strong floor, d) contoured bearing plate to distribute support reactions.

During a trial run of the cantilever setup large tip deflections were observed due to considerable and unstable rotation at the 'fixed' support. Furthermore, the force couple, which resisted the applied moment at the supported end of the beam initiated crushing of the concrete over the support – at which point the trial test was stopped. The crushing under the cantilevered support is shown in Figure 30.

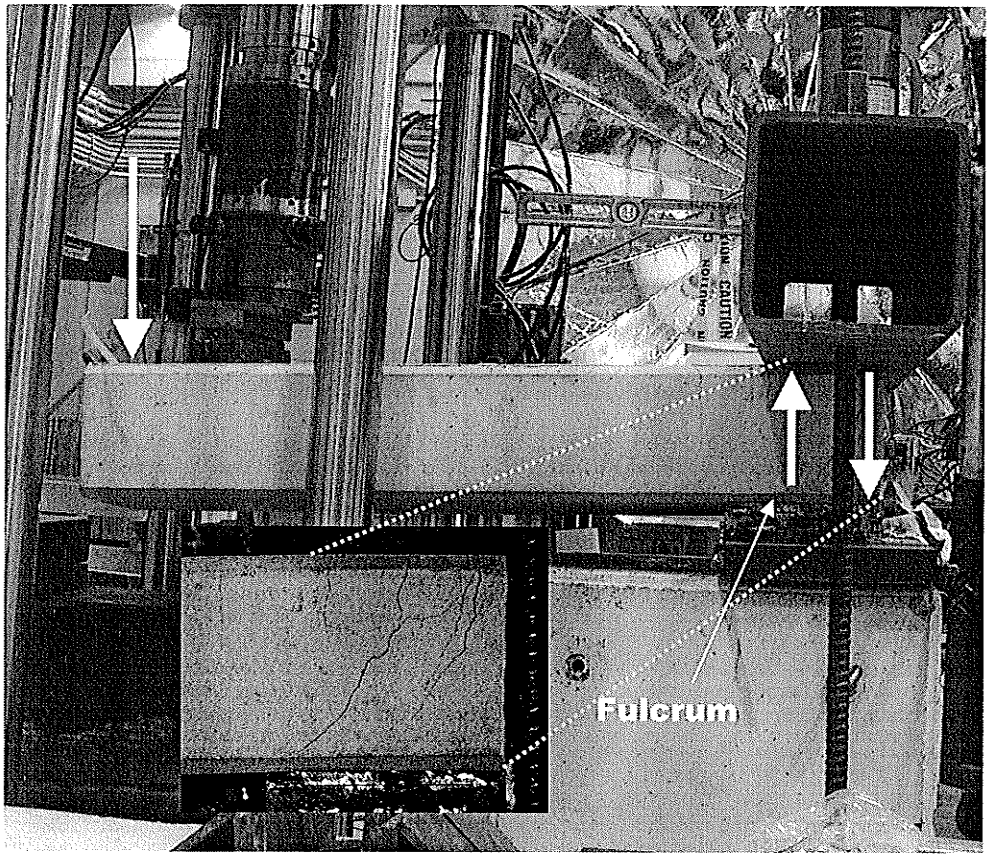

Figure 30. Force couple in cantilever support causing crushing of concrete.

After the unsuccessful performance of the cantilever setup, a simply supported system was designed to perform the bending tests. Since the test specimens are relatively short, when they are loaded at midspan in a simply supported configuration the a/d ratio that you can achieve is quite small for a bending test. This is why this type of setup, which is much easier to assemble, was not used from the start. The a/d ratio for the cantilever setup was 7.0 – well within the pure bending zone, while the simply supported setup had an a/d ratio of 3.5, which is less desirable because it falls in the combined bending and shear zone, therefore shear stresses may have a contributing role in the bending test. However, this compromise was more acceptable than the problems associated with the cantilever setup. Figure 31 shows the simply supported test setup that was used to perform the bending tests.

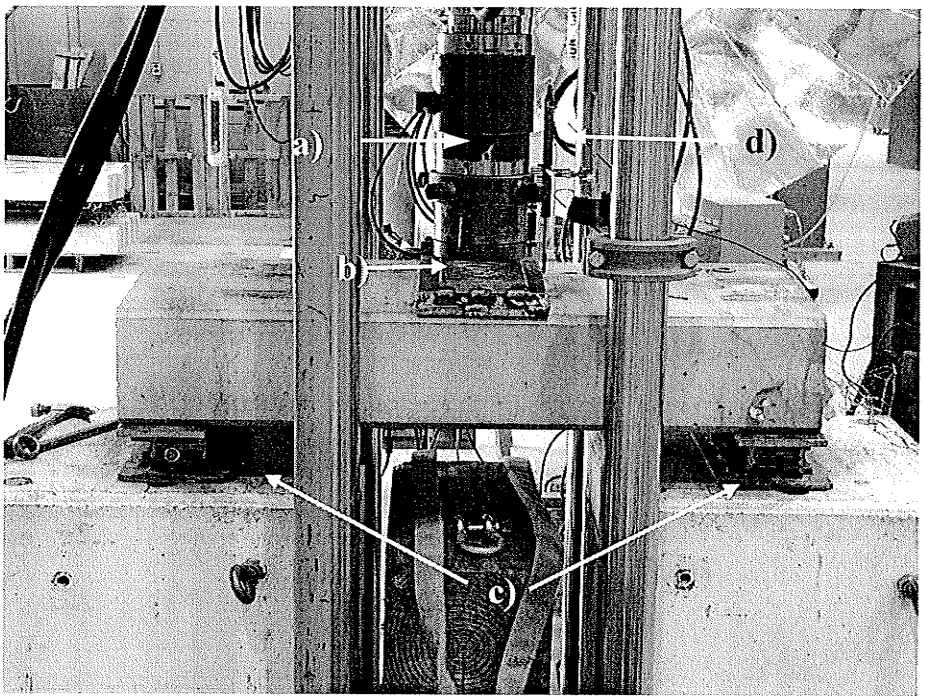

Figure 31. Simply supported bending test setup. a) actuator, b) contoured load plate, c) roller supports, d) LVDT to measure midspan deflection.

The bending test specimens were instrumented with six strain gauges mounted on internal reinforcement prior to casting. Two gauges were attached to the longitudinal reinforcement 275 mm from the end of the beam – originally thought to be near the point of maximum bending for the cantilever support setup. Four gauges were mounted on the vertical legs of the stirrups: two gauges were mounted on the second stirrup located approximately 150 mm from the end of the beam, and two gauges were placed on the third stirrup located approximately 250 mm from the end of the beam. In addition, an LVDT was used to record deflections at midspan, the location of maximum deflection.

6. RESULTS AND DISCUSSION

The following sections discuss the results from each test completed in the experimental testing program. The test results for the pullout test and the lateral test will be presented in brief. More details on these test results can be found in the Final Technical Report submitted for this project [Mufti et al, 2004].

6.1 Pullout Test

The first series of pullout tests were performed on beam specimens salvaged from Brookside Cemetery. A precast steel reinforced concrete beam cast with ordinary concrete in 1999/2000 was cut into six beam specimens, which yielded four pullout tests per beam specimen. The results from these pullout tests will be referred to as 'old mix' results. All others are referred to as 'new mix'.

Two types of mounting pins were evaluated in the pullout test: threaded stainless steel rods, and sand coated GFRP rods. All pullout rods were embedded in 152 mm deep holes in the concrete support beam specimens, which were filled with Hilti RE 500 epoxy. To analyze the bond performance of the pullout specimens the pullout force has been converted into average bond shear stress, u, as described in section 4.1.

6.1.1 Threaded stainless steel rods

Table 5 shows a summary of the results from the pullout tests with the threaded stainless steel rods. All of the specimens tested exceed the 22 kN minimum pullout capacity for field installation [Public Works Government Services Canada, 2003]. As can be seen from the data, the range of the ultimate pullout load is relatively small for each of the stainless steel specimens regardless of exposure to freeze/thaw cycles. Furthermore, the freeze/thaw cycles did not appear to have any significant

effect on the ultimate pullout load or the behaviour of the specimens. This can be attributed to the mode of failure most common with these specimens: as the pullout load was applied, concentric cracks appeared in the concrete around the embedded stainless steel pin, forming the typical cone-shaped failure surface associated with pullout failures. As the load increased these cracks widened until the stainless steel bars yielded and eventually failed. Although there was significant damage to the concrete, and a concrete pullout failure was in progress, the failure load was governed by the diameter of the stainless steel pin. Only one of the 26 stainless steel specimens experienced a concrete cone pullout failure without rupture of the steel bar. Figure 32 shows a typical failed stainless steel pullout specimen.

Table 5. Summarized pullout test results for stainless steel specimens.

Stainless Steel Pullout					
Exposure Conditions	Control		50 Cycles		250 Cycles
Concrete mix	Old mix	New mix	Old mix	New mix	Old mix
Number of Specimens	4	8	8	4	2
Mean Ultimate Pullout, $\overline{X}$ (kN)	97	104	99	101	103
Standard Deviation, σ (kN)	3.1	3.6	2.0	5.1	0.7
Range (kN)	94 -101	99 -108	96 -102	96 -108	103 -104

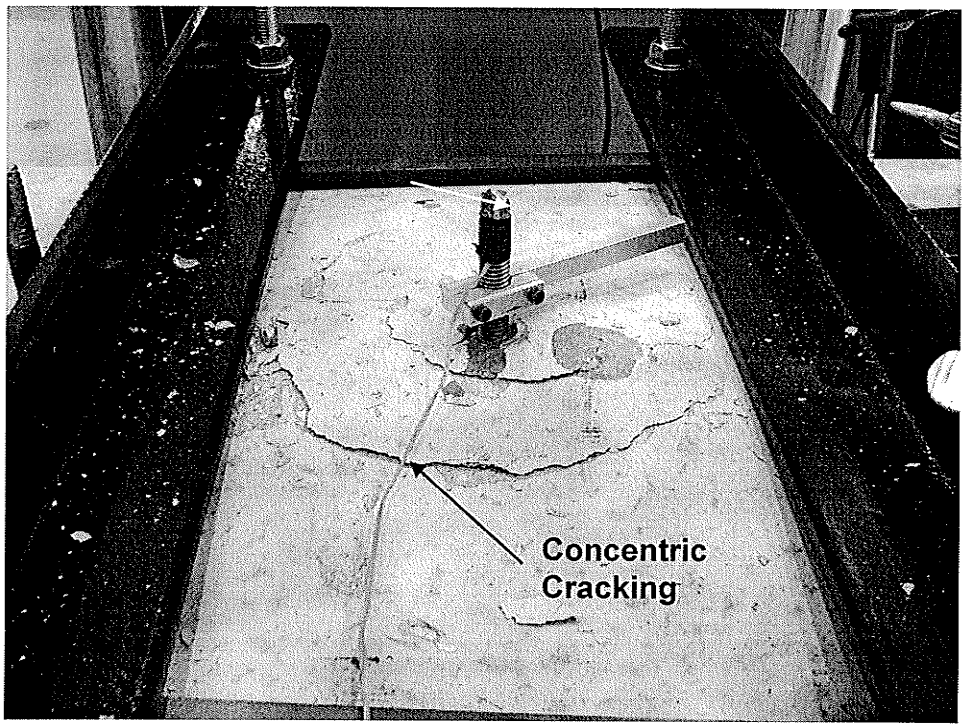

Figure 32. Stainless steel pullout specimen after typical yielding failure.

The pullout-slip behaviour of typical stainless steel pullout specimens is shown in Figure 33. Regardless of exposure to freeze/thaw cycles, the curve for the stainless steel specimens was similar to the general shape of the curve for the theoretical bond stress vs bond slip of an element of a reinforcing bar embedded in concrete (Figure 5). Generally, the amount of slip per unit pullout load is relatively small during the initial stages of loading and increases nonlinearly towards the final stages of loading. This means that when the bar is near failure a small increase in load will have a large increase in slip displacement.

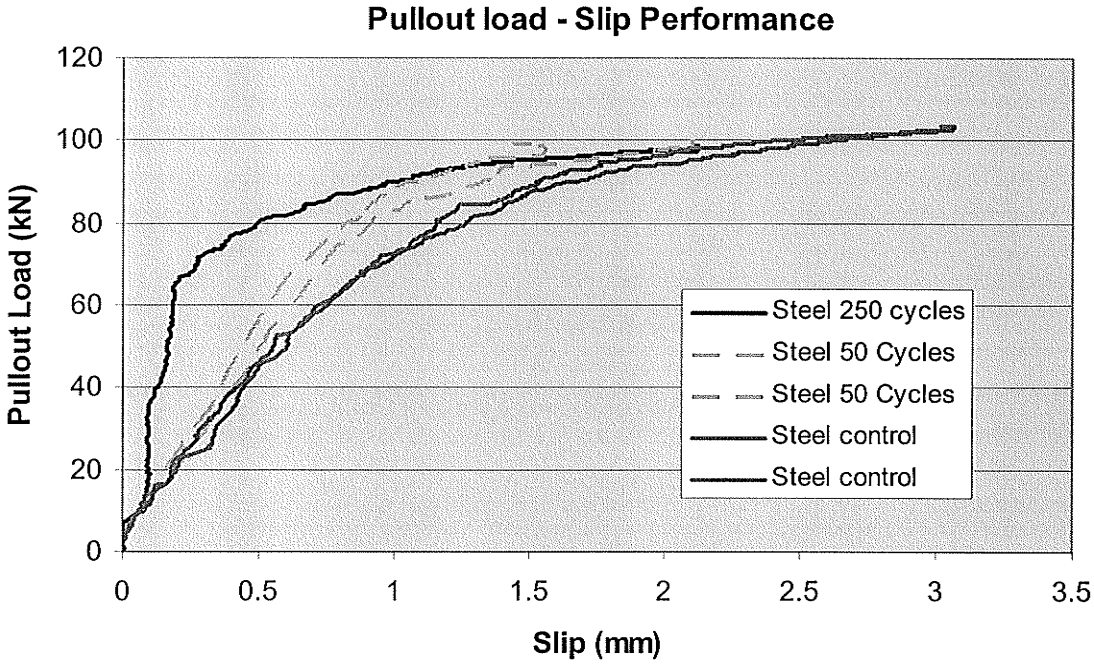

Figure 33. Load-slip behaviour of stainless steel pullout specimens.

Subsequent to pullout testing, specimens were cored and split to observe the state of the material interfaces after failure. Examination of the split cores confirmed that the slippage of the threaded stainless steel specimens that took place during testing occurred at the epoxy - concrete interface. No slippage could be detected at the steel – epoxy interface. This is due to the fact that the threaded stainless steel bars develop exceptional mechanical interlock when embedded in epoxy, thus slippage along this interface is unlikely. Figure 34 shows the split core of a typical stainless steel pullout specimen.

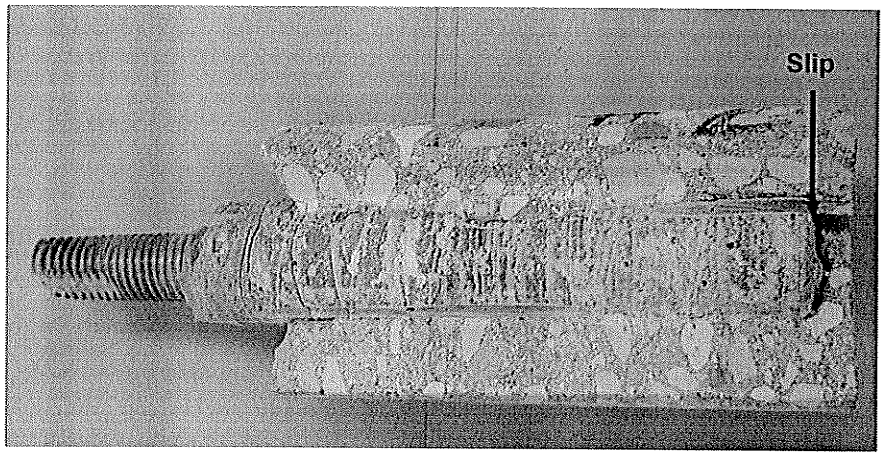

Figure 34. Typical slippage observed at epoxy – concrete interface.

6.1.2 GFRP rods

A summary of the results of the GFRP mounting pin pullout tests is shown in Table 6. Again, all of the specimens tested exceed the 22 kN minimum pullout capacity for field installation [Public Works Government Services Canada, 2003]. The experimental results indicate that there is no reduction in the pullout strength of the GFRP mounting pins with exposure to freeze/thaw cycles. In fact, the average pullout strength for the GFRP mounting pins appeared to increase with increased exposure to freeze/thaw cycles. Old mix beams had an average pullout load of 81 kN, 85 kN, and 111 kN for control, exposure to 50 cycles and exposure to 250 cycles respectively. Furthermore, new mix beams had an average pullout load of 61 kN and 89 kN for control and exposure to 50 cycles respectively. The most probable explanation for this apparent increase is that the matrix of GFRP rods have the tendency to absorb moisture [Liao et al, 1998; Helbling et al, 2002; Byars et al, 2001]; during cycling the relative humidity was held at 80%, and the surfaces of the pullout specimens were covered with 25 mm of water, which may have facilitated swelling of the GFRP rod and consequently an increase in the frictional component of the bond strength. Other possible explanations include increased moist curing time for the concrete of cycled specimens, increased setting time for the epoxy, and effects due to the post curing - which is a typical increase in strength of FRP

materials when exposed to high temperature (the +40 °C portion of the temperature cycle) for extended periods of time. More testing would be required to determine the cause of the increase in GFRP pullout strength with exposure to environmental conditioning, if it exists, with any certainty.

Table 6. Summarized pullout test results for GFRP specimens.

GFRP Pullout					
Exposure Conditions	Control		50 Cycles		250 Cycles
Concrete mix	Old mix	New mix	Old mix	New mix	Old mix
Number of Specimens	4	8	8	8	2
Mean Ultimate Pullout, $\overline{X}$ (kN)	81	61	85	89	111
Standard Deviation, σ (kN)	6.2	17.1	9.7	18	11.3
Range (kN)	74 -88	46 -94	73 -102	66 -117	104 - 120

The GFRP pullout specimens had a slightly different failure mode than the stainless steel pullout specimens. The cracking patterns on the GFRP specimens were similar to those observed on stainless steel specimens before failure, however, the ultimate load of the GFRP pin specimens was governed by slip behaviour. During testing, load was applied until the GFRP pins slipped vertically – usually only a few millimeters – and consequently the load would drop significantly. After a GFRP mounting pin had slipped, the peak load it reached before slipping could not be sustained again. If a specimen was reloaded after an initial slip, it would experience further slippage initiated at a lower load. Since a slippage type of failure is much less consistent than the yielding of steel pins, the pullout load range for the GFRP pins is much wider than for the stainless steel tests. A failed GFRP pullout specimen is shown in Figure 35.

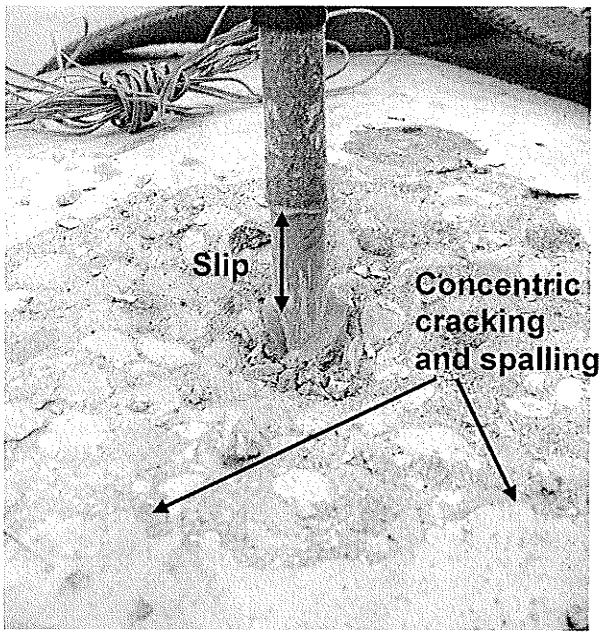

Figure 35. Typical slippage failure of GFRP pullout specimens.

The pullout load – slip performance for GFRP pullout specimens is shown in Figure 36. Since the performance of the GFRP pullout specimens is governed by a relatively inconsistent slippage failure, the pullout load – slip curves vary considerably from one another. Furthermore, no clear difference in the shape of the load – slip curves could be seen between the control and cycled specimens. However, one consistency between all the GFRP load – slip curves is that, similar to the stainless steel load – slip curves, they become more horizontal as the pullout load increases. This means that at loads nearing failure a small increase in load will have a larger increase in slip displacement.

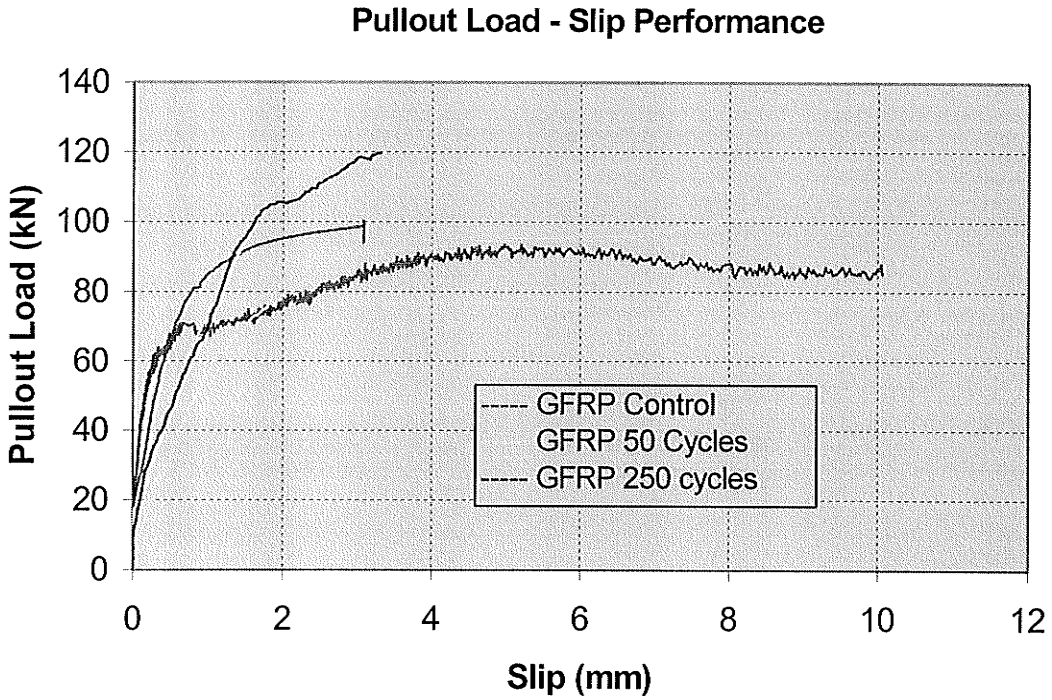

Figure 36. Pullout load – slip performance of GFRP pullout specimens.

Subsequent to pullout testing, GFRP pullout specimens were cored and split to observe the state of the material interfaces after failure. Examination of the split cores revealed that the slippage that took place during pullout testing occurred at the GFRP bar - epoxy interface. This implies that the bond strength between the GFRP bar and the epoxy is somewhat weaker than the bond strength between the stainless steel threaded rod and the epoxy. This is to be expected considering that the sand coated surface of the GFRP bars is much less pronounced than the steel ribs on the stainless steel threaded rod. Consequently, the mechanical interlock component, and thus the overall bond strength of the GFRP rod, is lower. Figure 37 shows a split core sample taken from a GFRP pullout test specimen.

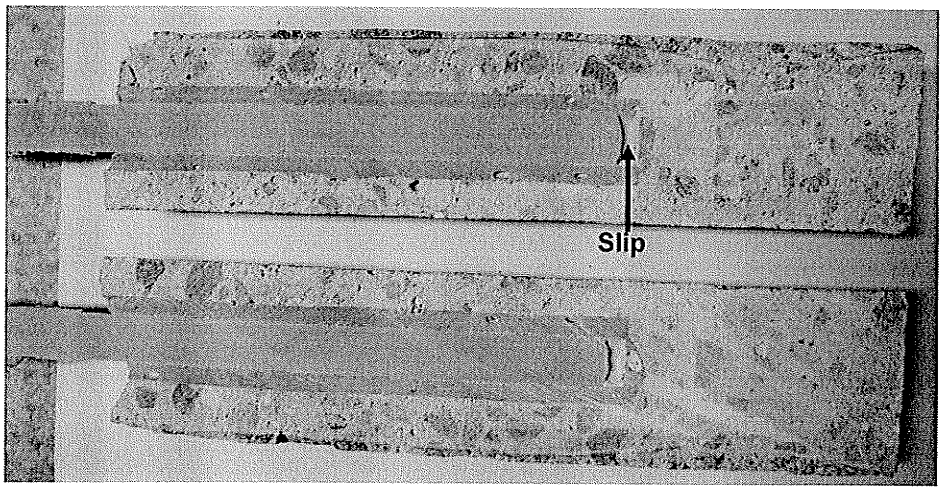

Figure 37. Typical slippage observed at the GFRP – epoxy interface.

6.2 Lateral Test

The lateral test was performed in order to determine the overall strength and behaviour of each marker mounting method. Three different marker mounting methods were evaluated using the lateral test: the pinning method, the pocket method, and the bumper method, as described in Section 5.2. As there were many variables under investigation and only a limited amount of time and resources available, several of the variable combinations had only one representative sample.

Lateral test results for the stainless steel pinned specimens, GFRP pinned specimens, pocket method specimens and bumper method specimens are shown in Tables 7, 8, 9 and 10 respectively. All of the specimens tested exceeded the 1 kN of lateral resistance required for field installation [Public Works Government Services Canada, 2003].

Table 7. Lateral test results for markers attached with stainless steel pins.

Pinned Method (stainless steel pins)						
Pin length and material	305 mm Stainless steel				152 mm Stainless steel	
Exposure	Control		50 Cycles		Control	
Granite	St.	Bar.	St.	Bar.	St.	Bar.
Number of specimens	1	1	4	1	2	-
Failure load range (kN)	5.4*	8.9*	4.7 – 6.6	8.5*	5.0 – 5.2	-
Top displacement range at max load (mm)	31.2*	62.4*	21 - 33	51*	13 - 14	-

St. = Stanstead granite, Bar. = Barre granite. *Only one sample available.

Table 8. Lateral test results for markers attached with GFRP pins.

Pinned Method (GFRP pins)						
Pin length and material	305 mm GFRP				152 mm GFRP	
Exposure	Control		50 Cycles		Control	
Granite	St.	Bar.	St.	Bar.	St.	Bar.
Number of specimens	1	1	4	1	2	2
Load range (kN)	5.5*	6.6*	4.5 – 6.7	6.9*	4.6 – 4.9	4.5 – 4.9
Top displacement range at max load (mm)	45.2*	41.0*	34 - 52	45.1*	22 - 30	27 – 24

St. = Stanstead granite, Bar. = Barre granite. *Only one sample available.

Table 9. Lateral test results for markers attached by the pocket method.

Pocket Method				
Exposure	Control		50 Cycles	
Granite	St.	Bar.	St.	Bar.
Number of specimens	3	3	5	1
Load range (kN)	4.5 – 4.9	5.9 – 6.4	3.0 – 4.8	5.1*
Top displacement range at max load (mm)	3.4 – 4.0	3.4 – 3.6	3.3 – 4.9	3.8*

St. = Stanstead granite, Bar. = Barre granite. *Only one sample available.

Table 10. Lateral test results for markers attached by the bumper method.

Bumper Method				
Exposure	Control		50 Cycles	
Granite	St.	Bar.	St.	Bar.
Number of specimens	3	3	5	1
Load range (kN)	3.0 – 5.0	3.8 – 6.9	3.3 – 5.3	5.6*
Top displacement range at max load (mm)	3.4 – 5.3	2.6 – 5.1	4.0 – 7.8	6*

St. = Stanstead granite, Bar. = Barre granite. *Only one sample available.

The pinned specimens behaved similarly to a reinforced concrete beam, where compressive stresses are taken by the concrete, or in this case granite, and tensile stresses are taken by internal steel or GFRP reinforcement. For this reason, the pinned granite markers failed just above where the stainless steel or GFRP mounting pins ended – the point where the granite had to resist tensile stress without reinforcement. Therefore, the pinned specimens generally resisted higher

loads than the pocket or bumper methods because these methods have no reinforcement to resist the tensile forces at the base of the marker where these bending stresses are highest. For example, the failure load range for cycled Standstead granite - stainless steel pinned, GFRP pinned, pocket, and bumper specimens were 4.7 – 6.6 kN, 4.5 – 6.7 kN, 3.0 – 4.8 kN, and 3.3 – 5.3 kN respectively. Clearly the use of marker mounting pins increases lateral strength. Figures 38, 39 and 40 show failed pinned, pocket and bumper specimens respectively.

As expected, the specimens attached with 152 mm pins had slightly lower failure load ranges than the specimens attached with 305 mm pins. For example GFRP pinned control specimens with Standstead granite markers had a failure load range of 4.5 – 4.9 for 152 mm pins, while the control specimen with 305 mm pins had a failure load of 6.6 kN. Similarly, the stainless steel pinned control specimens with 152 mm mounting pins had a failure load range of 5.0 – 5.2 while the control specimen with 305 mm pins had a failure load of 5.4 kN.

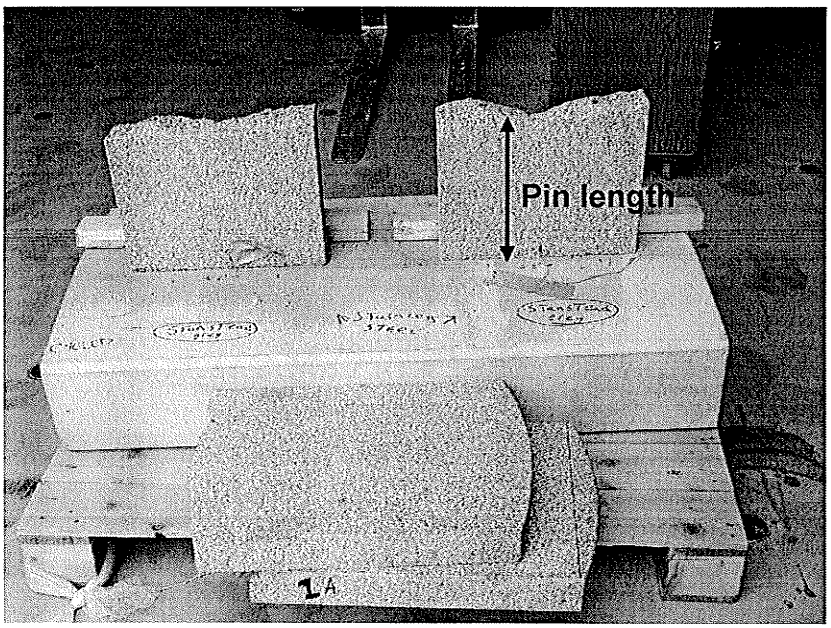

Figure 38. Failed stainless steel pinned specimens –marker failed just above end of mounting pin.

Figure 39. Failed pocket specimen – marker failed flush with support beam.

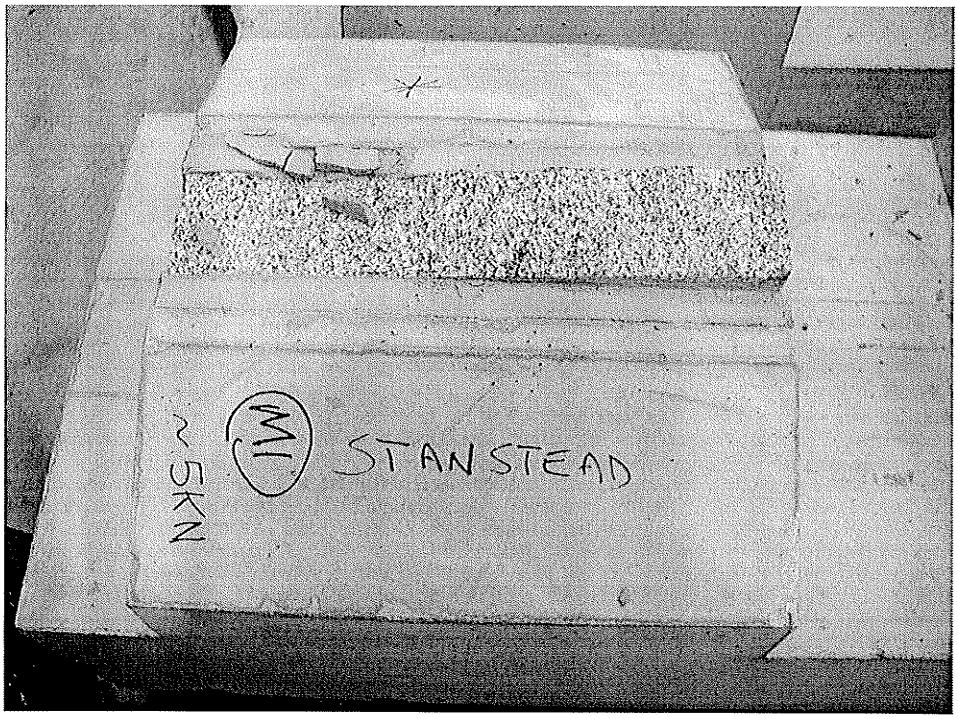

Figure 40. Failed pocket specimen –marker failed flush with concrete bumpers.

A large difference in strength was observed between the marker granite types. Marker mounting assemblies that used Barre granite markers had consistently higher failure loads than those using Standstead granite markers. For example, pocket method control specimens had a failure load range of 4.5 – 4.9 kN and 5.9 – 6.4 kN for Standstead and Barre granite respectively.

The freeze/thaw cycles did not appear to have any significant effect on either the pinning or bumper methods. However, there was a slight decrease in the failure load range of the markers mounted by the pocket method after exposure to freeze – thaw cycles. Control pocket method specimens with Standstead granite markers had a failure load range of 4.5 - 4.9 kN while cycled specimens had a load range of 3.0 – 4.8 kN. Similarly the control pocket specimens with Barre granite markers had a failure load range of 5.9 - 6.4 kN while the cycled Barre granite specimen had a failure load of 5.1 kN. It is hard to say whether this apparent trend was due to a lack of a sufficient number of specimens, or if the pocket method is indeed highly susceptible to freeze/thaw degradation. It should be noted however, that none of the specimens experienced any visible cracking after freeze/thaw conditioning.

The pinning method provides a much more flexible connection than the pocket or bumper methods. Since the pocket and bumper methods are completely rigid connections, they allow very little movement before failure. This may arise as a serviceability issue if the markers are intended to withstand and absorb accidental impact without failure. Figure 41 shows a comparison of the lateral load – lateral maker deflection behaviour for stainless steel pinned, GFRP pinned, pocket, and bumper method specimens.

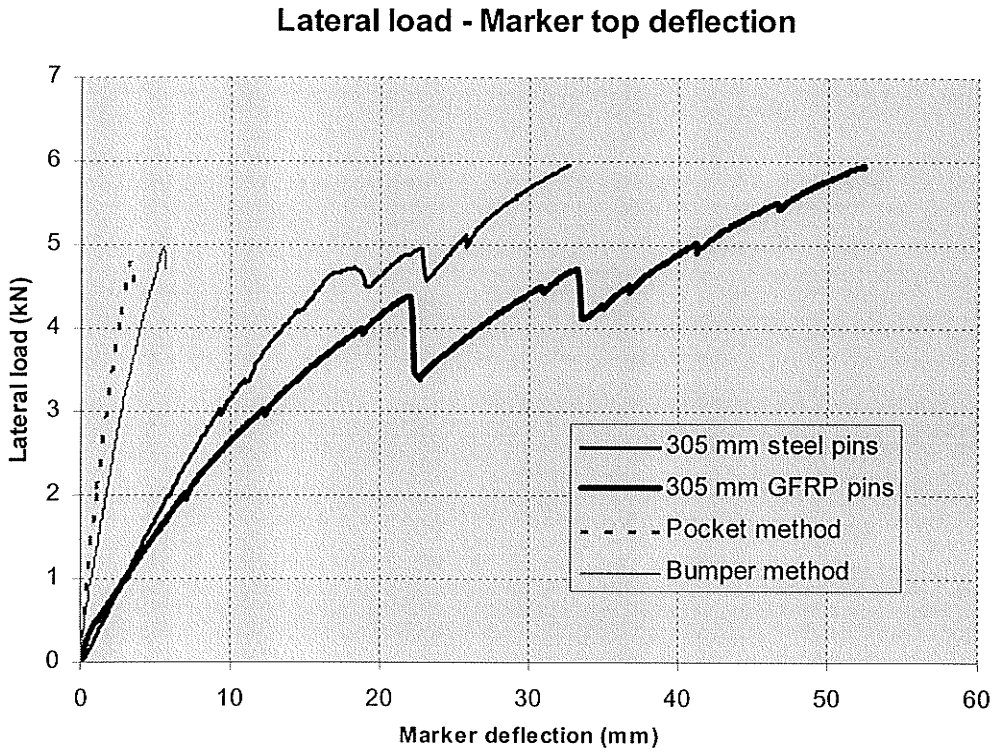

Figure 41. Typical lateral load – marker deflection behaviour for cycled lateral test specimens with Standstead granite markers.

All but four of the lateral test specimens failed by complete cracking of the granite marker. Of these four specimens, two were Barre granite pinned with 305 mm GFRP pins, one was Barre granite pinned with 152 mm GFRP pins, and one was Stanstead granite pinned with 152 mm stainless steel pins. In these cases, the markers developed high lateral deflection followed by minor cracking (and in the case of the 152 mm stainless steel pin, developed severe crushing of granite near the base of the marker) but did not break. An example of a lateral test specimen withstanding large lateral deflection is shown in Figure 42.

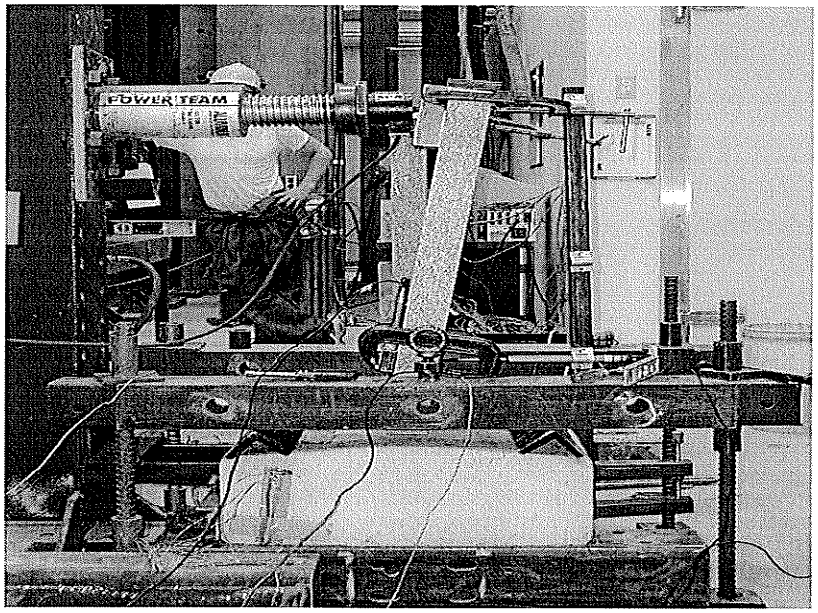

Figure 42. Barre granite marker pinned with 305 mm GFRP pins sustaining significant lateral deflection.

The lateral tests of the four specimens that did not fail by complete cracking of the granite marker ended in two different ways. Two of the specimens experienced significant deflection, followed by a sudden drop in load after an audible cracking or popping noise. In these cases, the failure mode was assumed to be due to slippage of the mounting pin. Observation of the split core of these specimens showed no slippage at the connection of the mounting pin to the support marker. Therefore, it appears that the slippage occurred in the epoxied connection between the granite marker and the protruding mounting pins. The other two lateral tests ended when the maximum stroke of the hydraulic jack had been reached, and the test could not continue. In these four cases, when the load was removed the markers experienced a 'recoil' effect and returned to their original position relatively undamaged. As expected, more damage was observed on the Standstead granite marker that experienced the recoil effect than was observed on the Barre granite markers. Figures 43 and 44 show Barre granite and Standstead granite specimens that experienced the recoil effect after the lateral load was removed.

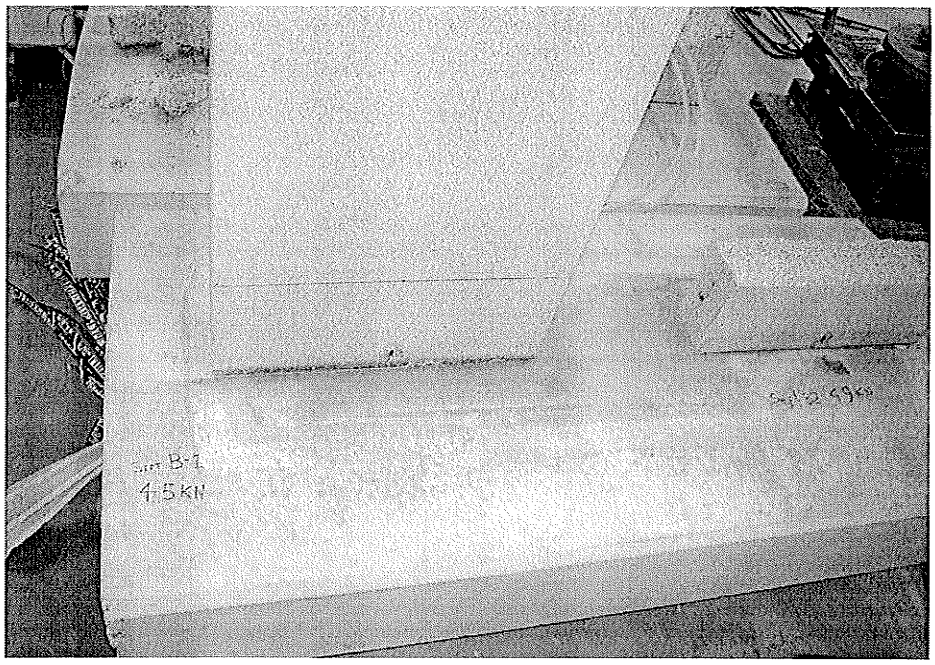

Figure 43. Barre granite marker virtually undamaged after lateral load was removed.

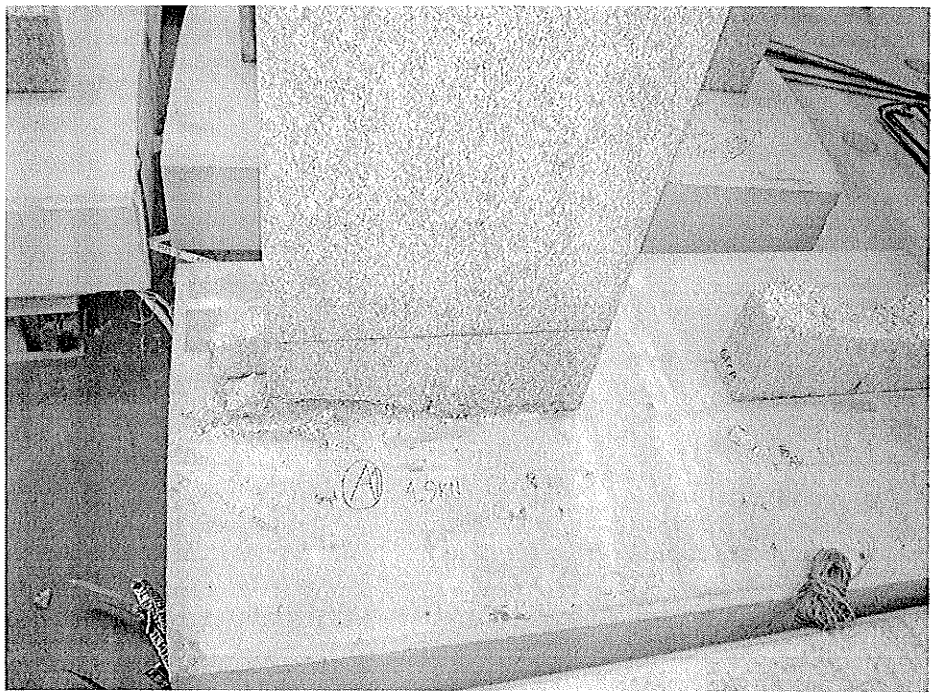

Figure 44. Standstead granite marker that experienced the recoil effect sustained significant crushing of granite.

It is interesting to note that only one of the lateral test specimens that employed both a Barre granite marker and GFRP mounting pins failed by complete cracking of the granite marker. The other three specimens with the same granite/GFRP combination experienced the more desirable recoil effect. It appears that the combination of Barre granite markers pinned with GFRP mounting pins is most likely to produce this more desirable behaviour.

6.3 Shear Test

Six specimens were used in the shear investigation of the support beam; two were reinforced with steel and four were reinforced with GFRP. One steel specimen and one GFRP specimen were subjected to the simultaneous shear stress and freeze/thaw conditioning program as described in section 5.6.3.2. This specimen data has been compiled in Table 11, and the results from the shear testing program are shown in Table 12. The failure loads have been converted to shear forces at failure by multiplying the failure load by the distance to the far end of the beam and dividing by the total length of the beam. The results have also been display graphically for ease of comparison in Figure 45.

Table 11. Shear test specimens.

Reinforcement	Total number of specimens	Number of conditioned specimens	Number of control specimens
GFRP	4	1	3
Steel	2	1	1

Table 12. Shear test results.

Reinforcement	Condition	Failure Load (kN)	Failure Shear Force (kN)
GFRP	Control	370	289
	Control	366	286
	Control	370	289
	Cycled	345	270
Steel	Control	525.7	411
	Cycled	480	375

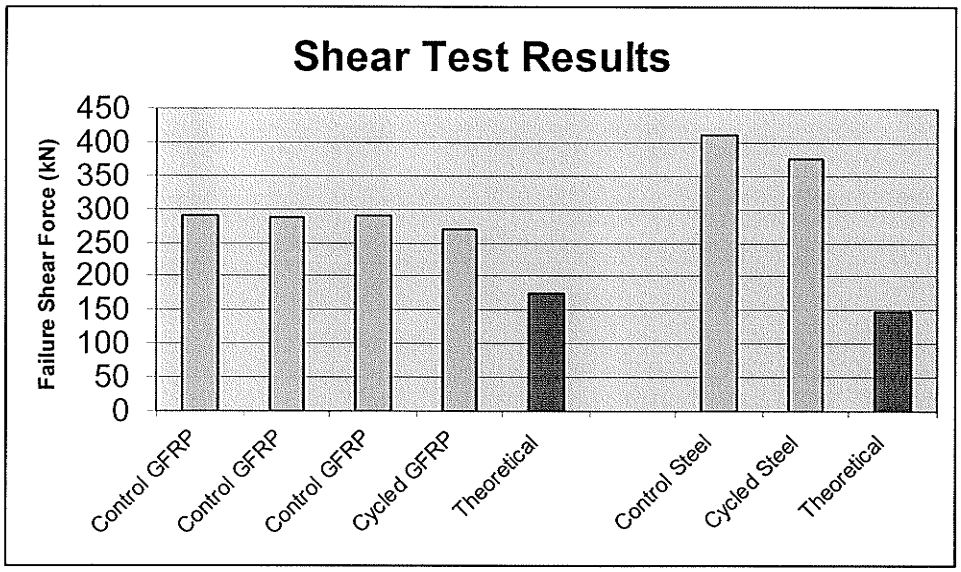

Figure 45. Shear test results.

As can be seen from Figure 45, the steel reinforced specimens had a slightly higher shear capacity than the GFRP specimens; however, the actual failure shear loads for each specimen were several times larger than those predicted by calculation (148 kN and 176 kN for steel and GFRP reinforced specimens respectively). This is probably because the design calculations used to predict the shear capacity of the

specimens only incorporate the shear resistance contribution from the uncracked concrete and the shear reinforcement (stirrups). In reality, there is diagonal interface shear resistance, which is the result of interlock and friction along shear cracks, and dowel action of the longitudinal reinforcement that also contribute to the overall shear capacity of a section. The component of interlock and shear friction decreases as shear cracks widen under increased deflection. This may lead to an explanation as to why the GFRP reinforced specimens had slightly lower failure loads; since the GFRP reinforced sections are less stiff than the steel reinforced specimens, they deflect further under the same load. This creates wider cracks, which reduces shear friction and interlock, resulting in a reduced ultimate shear capacity. A failed shear test specimen with distinct shear cracks is shown in Figure 46.

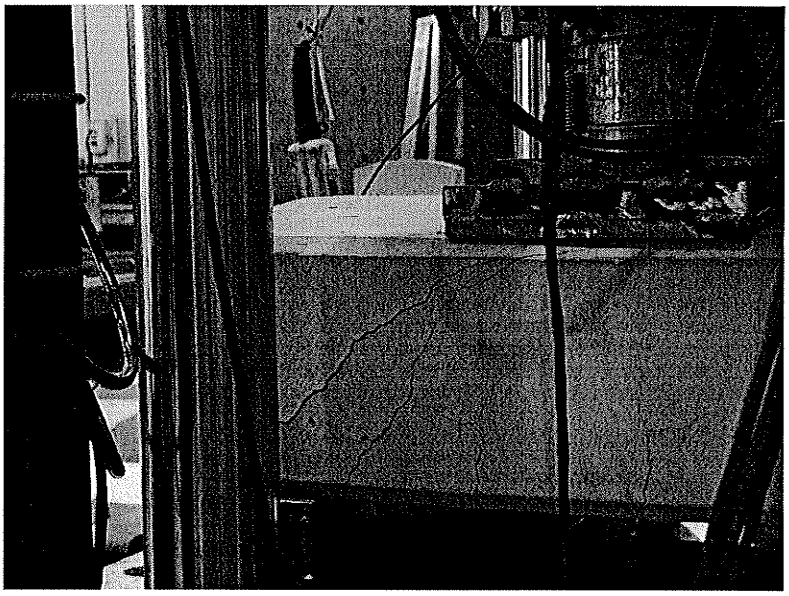

Figure 46. Typical failed shear test specimen.

Regardless of the type of internal reinforcement used, each specimen tested had well over ten times the capacity required to resist design shear loads (V_f = 23 kN). It is very unlikely that the shear capacity of either of the support beam designs will ever be exceeded under normal service conditions.

The GFRP and steel reinforced specimens that were subjected to the environmental conditioning program had slightly lower failure loads than control specimens. However, these differences were so small that they can be deemed insignificant. Many more samples, and exposure to increased numbers of freeze/thaw cycles, would be required to determine if the environmental conditioning program has any negative impact on the shear performance of the support beam specimens.

No meaningful observations or comparisons could be made from the data collected from the strain gauges mounted on the internal reinforcement of the shear test specimens. The strain gauges mounted on the stirrups recorded either large and positive strains, large and negative strains, or nearly zero strain throughout the test with no clear pattern as to what caused the particular behaviour. The poor quality of the data from these gauges may be attributed to two factors. First, the stresses generated inside a member subjected to high shear loads are very complex and variable – especially with an a/d ratio as low as 1.75 – and cannot be easily predicted. Since the gauges were located within this discontinuous zone of high stress, the data is much more inconsistent. Moreover, as previously discussed, there are several components that contribute to a member's overall shear capacity (concrete strength, friction and interlock, stirrups, and dowel action). The contribution from each of these components varies throughout a test as stresses are redistributed when cracks develop throughout different regions in the member. This makes meaningful comparisons of data between specimens very difficult. Secondly, the reliability of the strain gauges could be called into question. There is great potential for gauges mounted on internal reinforcement to become damaged during the casting procedure, as well as during the almost 1.5 years the gauges spent inside the specimens from the time of casting to testing. The strain data generated by these gauges will not be discussed in this report, however load – strain curves for each shear specimen have been plotted and can be found in Appendix A.

Due to the large variation in the data from the internally mounted strain gauges, the analysis of the shear tests will focus on the data generated using the LVDTs. Figure 47 shows a comparison of the load – defection behaviour for each shear test specimen.

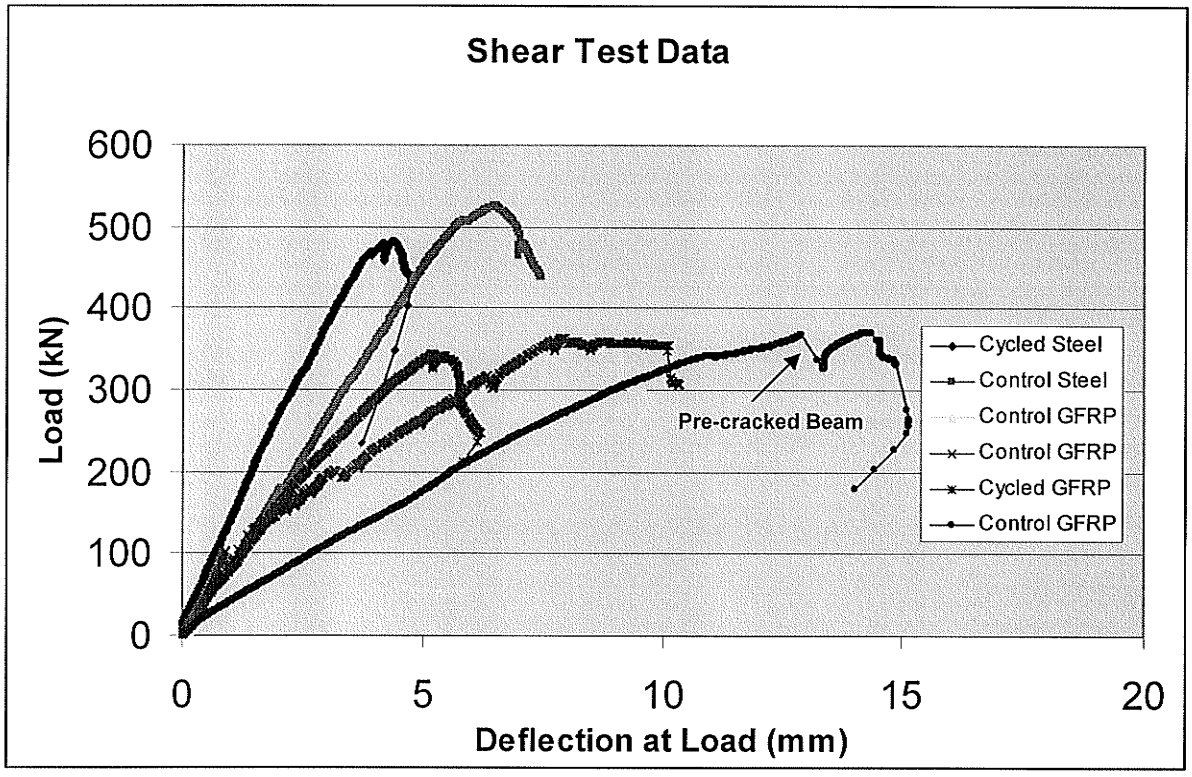

Figure 47. Load – deflection behaviour of shear test specimens.

As seen in Figure 47, the GFRP reinforced specimens were less stiff than the steel reinforced specimens, as expected. Furthermore, the specimens subjected to the environmental conditioning program appeared to be slightly stiffer than control specimens. It is unlikely that this small difference in stiffness can be attributed to the effects of the environmental conditioning program, and much more likely that this is due to normal variation between test specimens. One of the GFRP reinforced specimens was damaged during a trial test of the original apparatus used to apply shear stress in the environmental chamber. This damaged specimen was salvaged

and shear tested and has been labelled 'pre-cracked' on the load – deflection curve. As expected the pre-cracked specimen has significantly less stiffness than the other shear test specimens, although its ultimate capacity appears to be unaffected by the prior damage.

6.4 Bending Test

Five specimens were used in the bending investigation of the experimental program; two were reinforced with steel and three were reinforced with GFRP. One steel reinforced specimen and one GFRP reinforced specimen were subjected to combined bending stress and freeze/thaw cycles, as described in section 5.6.3.1, the others were used as control specimens. The specimen information and the results of the bending tests are shown in Table 13. The failure load has been converted in to a failure moment by multiplying the failure load by the distance between supports and dividing by 4.

Table 13. Bending test results.

Reinforcement	Condition	Failure Load (kN)	Corresponding Bending Moment (kNm)
GFRP	Control	270	72.0
	Control	271	72.3
	Cycled	301	80.3
Steel	Control	389	103.8
	Cycled	445	119

The actual bending moments achieved during testing were comparable to predicted values. The calculated moment resistance for the support beam specimens (with

material resistance factors set to 1.0) was 80 kNm and 76 kNm for GFRP and steel reinforced specimens respectively. Two GFRP reinforced specimens failed slightly below the expected moment and one specimen failed at exactly the predicted value. The two lower failure moments could be attributed to variability in specimens/materials, or possibly, the shear stress generated from the relatively small a/d ratio of the test setup played a role in the premature failure of the specimens. Both of the steel reinforced specimens failed above the predicted failure moment. Again, this could be attributed to variations in material strengths, or perhaps the superior shear resistance of the steel reinforced specimens (as noted in Section 6.3) was responsible for the higher capacity. However, it is difficult to make any absolute conclusions about the bending performance of these specimens with so few specimens.

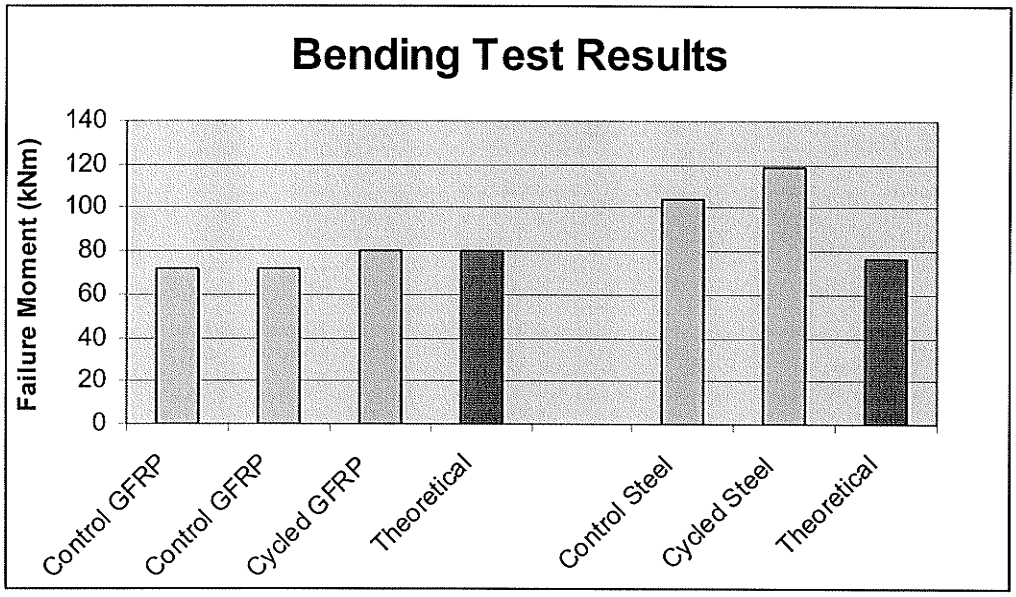

Figure 48. Bending test results.

As can be seen from Figure 48, the simultaneous exposure to sustained stresses and freeze/thaw cycles had no negative impact on the ultimate bending capacity of either the GFRP or Steel reinforced bending test specimens. In fact, the cycled specimens appeared to have slightly higher failure loads than control specimens.

There is no reasonable explanation for this trend and the differences are so small that it is most likely due to expected variations between specimens.

Figure 49 shows a typical failed bending test specimen. As expected, flexural cracks developed near the beginning of the test and could be seen almost throughout the entire section; however, near the end of the test shear cracks also developed and were quite substantial at failure. Again, this is due to the relatively low a/d ratio of 3.5, which puts this specimen into the combined shear and bending failure zone. It is difficult to say what influence the presence of these significant shear stresses had on the bending capacity of the specimens.

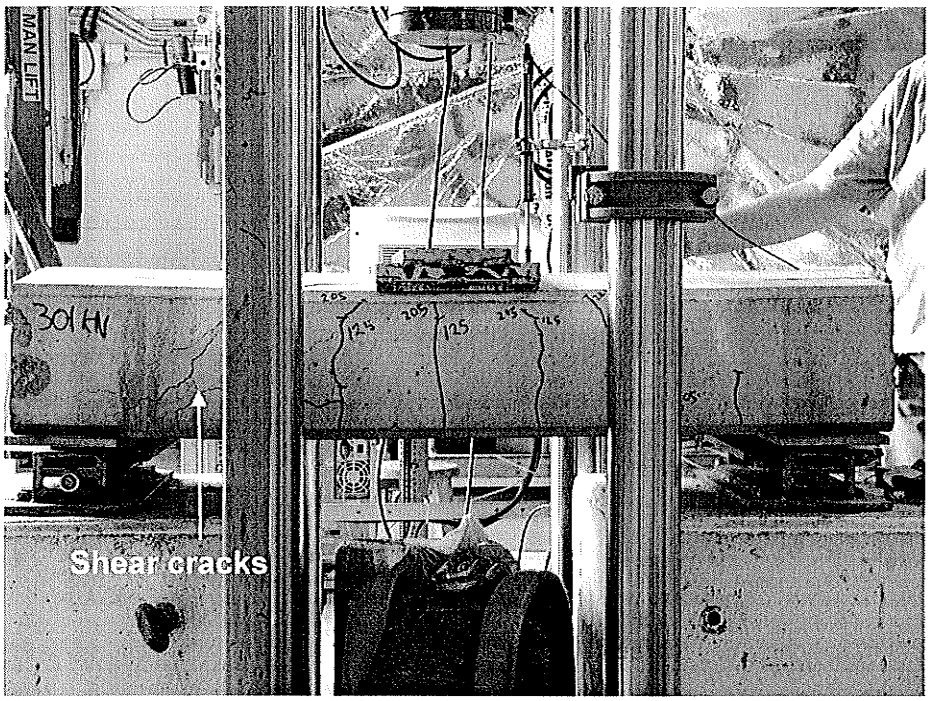

Figure 49. Typical bending test failed specimen.

As with the shear tests, the strain gauge data acquired during the bending test could not be used to gain any meaningful insight into the bending performance of the specimens. Again, the redistribution of shear stresses that occurs during testing makes the data from the strain gauges mounted on the stirrups difficult to use for

any kind of practical comparison. The data collected from the gauges mounted on the longitudinal reinforcement was also quite variable and not particularly useful for comparison. Notwithstanding, the load – strain behaviour for each bending test specimen has been plotted and is available for reference in Appendix B.

An LVDT was used to record the midspan deflection of the beams during testing and the data for each bending test specimen has been plotted in Figure 50. As expected, the steel reinforced specimens were significantly stiffer than the GFRP reinforced sections. It can also be seen that the specimens subjected to the conditioning program appeared to have slightly higher stiffness than control specimens, however this is unlikely an effect of the conditioning and can most likely be attributed to expected variation between specimens.

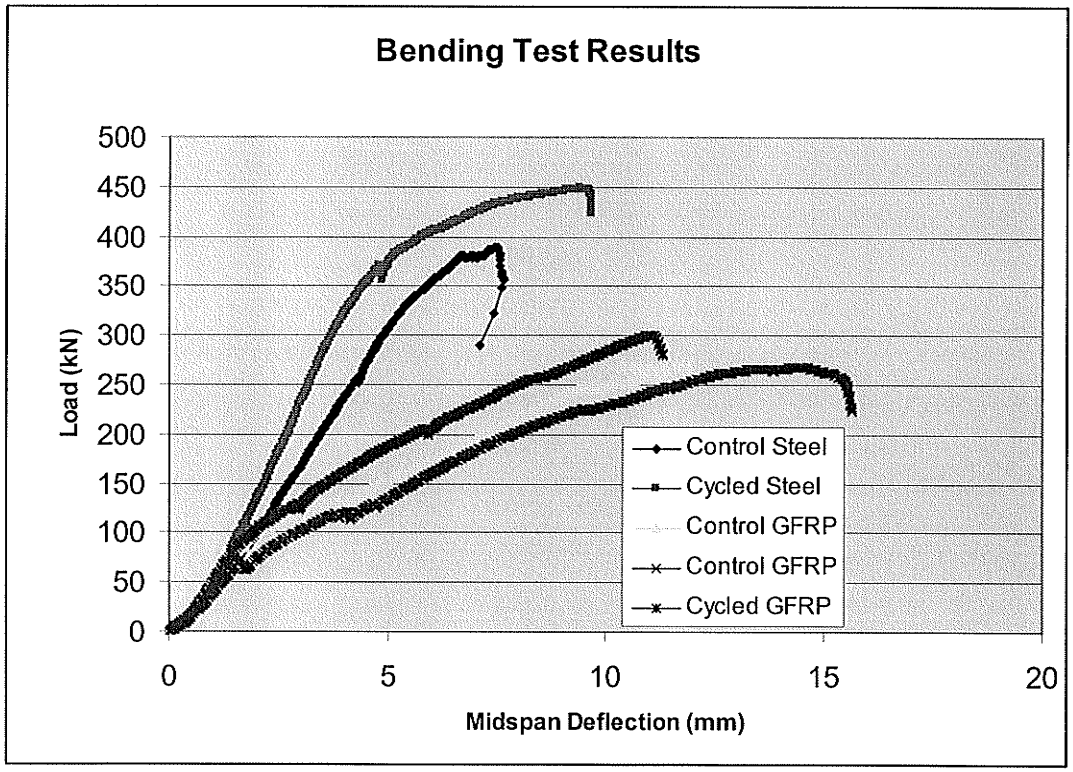

Figure 50. Load – deflection behaviour for bending test specimens.

7.0 CONCLUSIONS AND RECOMMENDATIONS

Mounting pin pullout tests and lateral tests were performed on various marker mounting assemblies to assist in selecting a new marker mounting design for use at Brookside Cemetery and other Canadian military cemeteries. The new marker mounting methods were tested after accelerated conditioning in a freeze and thaw chamber to evaluate the durability of the new designs.

The results of the pullout tests indicated that stainless steel mounting pins were not noticeably affected by 50 or 250 freeze and thaw cycles. Since the failure mode of these specimens was governed predominantly by the yielding of the pins, the failure loads were very consistent and had a relatively small range. Each stainless steel pullout specimen tested failed at loads well above the 22 kN required for field installation.

The GFRP mounting pin pullout results had a wider pullout load range than the steel pins, as the slippage failure that governed this design is more variable than a yielding type failure. This variability could be reduced by improving the bond of the sand coating on the GFRP bar, which would reduce the likelihood of slippage. However, since most of the slippage occurs at loads well above the 22 kN required for field installation, there is little worry of slippage failures being a concern for grave markers under normal service conditions. Furthermore, this system appeared to have an increase in strength with an increase in exposure to freeze and thaw cycles. Currently, this trend is not fully understood. It may be attributed to increased concrete curing and epoxy setting time or due to a swelling of the GFRP as it absorbs ambient moisture during conditioning, but further investigation would be required to fully understand this behaviour. Each GFRP pullout specimen tested failed at loads well above the 22 kN requirement. In all cases, the 152 mm (6") mounting pin specimens performed adequately, but not as well as the 305 mm (12") mounting pin specimens.

The lateral tests suggested that, in the absence of corrosion, the granite marker is the weakest component in the marker mounting assembly. Regardless of what mounting method is used; pinning, pocket, or bumper, the granite marker will always be the first component to fail. Overall the tests show that the pinning method was between 20% - 30% stronger than the other methods, due to the mounting pins acting like flexural reinforcement in a beam. The pinning and bumper methods were not affected by freeze and thaw conditioning; however the pocket method may have been slightly affected. Further testing would be required in order to determine the extent of these effects, if any, with more confidence. Furthermore, each of the specimens tested failed well above the 1 kN minimum requirement for field installation.

Three of the four lateral test specimens with GFRP pins and Barre granite markers experienced a flexible recoil effect – the marker returned to its original position virtually undamaged when the lateral load was removed. This is a desirable behaviour which allows the structural system to resist and absorb impact loads that it may encounter. One specimen with stainless steel pins also experienced this recoil effect; however, the granite marker was severely damaged after recoil. Furthermore, economics are also an important factor in the comparison of the mounting pin materials: stainless steel pins are several times more expensive than the GFRP pins, which make them less viable to implement.

Shear and bending tests were performed on support beam specimens reinforced with steel or GFRP to assist in selecting a new support beam design for VAC. The support beam specimens were tested after accelerated environmental conditioning consisting of simultaneous exposure to sustained stresses and freeze/thaw cycles.

The steel reinforced specimens had slightly higher ultimate shear strengths than the GFRP reinforced specimens, but each specimen tested had more than ten times the required shear resistance to resist design shear loads. The results from the shear

tests for both GFRP and steel reinforced specimens were well above predicted calculated values. This has been attributed to the presence of frictional and interlock forces acting between shear cracks that contribute to shear resistance, but are not considered in design calculations.

The GFRP and steel reinforced shear specimens that were subjected to the environmental conditioning program had slightly lower ultimate shear strengths than control specimens. However, these differences were very small and are most likely due to a reasonable variation between test specimens.

The bending test results were comparable to those predicted by calculation. The GFRP reinforced specimen results were slightly lower than expected and the steel reinforced specimen results were slightly higher than expected. These deviations from expected values could simply be the result of variation within the small sample size, or they may be the result of the effects of the shear stress influencing the bending capacities of the specimens. The bending specimens generally failed in a combined shear and bending state, where both flexural and shear cracks were present at failure. The presence of shear forces was unpreventable due to the relatively short length of the specimens.

The GFRP and Steel reinforced bending specimens that were exposed to sustained bending stress and freeze/thaw cycles appeared to have slightly higher failure loads than the control bending specimens. It is unlikely that the environmental conditioning improved their performance, and much more likely that this trend is the result of variation between specimens.

Overall, the results from each test show that GFRP mounting pins and reinforcement could be used as a viable and durable alternative to the current steel reinforced design. Although some of the tests showed higher ultimate strengths for the

specimens designed using steel materials, in all cases the specimens using GFRP were able to perform well above all requirements for field installation.

It is important to note that the GFRP reinforcement scheme for the support beam specimens used in this study were designed for ultimate limit states in laboratory conditions (i.e., all material resistance factors were set to 1.0) and not designed for use in service. Before a GFRP reinforced support beam could be implemented for use at Brookside Cemetery, the amount of reinforcement used would have to be adjusted to account for material resistance factors and serviceability limit states such as maximum allowable deflection criteria. However, once the effectiveness of using GFRP reinforcement in support beams has been established through an experimental program, the redesigning of the amount of GFRP reinforcement required to satisfy applicable design codes is a relatively simple process.

After consideration of all the test results, the respective behaviour of each system during testing, and the degree of corrosion resistance of each design, results indicate that a marker mounting assembly consisting of 305 mm (12") GFRP mounting pins and a Barre granite marker, supported on a GFRP reinforced support beam would be the most appropriate system for long-term field application.

REFERENCES

Almusallam, T.H., Al-Salloum, Y.A., Alsayed, S.H., Alhozaimy A.M.; Tensile Strength of GFRP Bars in Concrete Beams Under Sustained Loads at Different Environments; CDCC 2002.

Alsayed, S. H., Alhozaimy, A.M., Al-salloum, Y.A. and Almusallam, T.H.; Durability of the New Generation of GFRP Rebars Under Severe Environments; CDCC 2002.

ASTM C- 666 (1997); Standard Test Method for Resistance of Concrete to Rapid Freezing and Thawing, 1997.

ASTM E- 1512 (1993); Standard Test Method for Testing Bond Performance of Adhesive-Bonded Anchors, 1993.

ASTM E- 488 (1996); Standard Test Method for Strength of Anchors in Concrete and Masonry Elements, 1996.

B. Benmokrane; Bond Strength of FRP Bars Embedded in Concrete Beams; Proceedings, Annual Conference, Canadian Society for Civil Engineering; 1997.

Benmokrane, B., Rahman, H., Ton-That, M. and Robert, J.; Improvement of the Durability of FRP Reinforcements for Concrete Structures; CDCC 1998.

Benmokrane, B., Xu, H. and Bellavance, E.; Bond Strength of Cement Grouted GFRP Anchor Bolts; International Journal of Rock Mechanics, Vol. 33(5), 1996.

Byars E, Waldron P, Valter D and Sotiris, D.; Durability of FRP in Concrete Deterioration Mechanisms. FRP Composites in Civil Engineering; Vol. II; 2001.

CHBDC; Canadian Highway Bridge Design Code. Canadian Standards Association International. Toronto, Ontario, Canada. 2000.

Concrete Design Handbook A23.3 - Canadian Portland Cement Association - CSA Standard A23.3-94, Second Edition, 1998.

Ehsani, M.R., Saadatmanesh, H. and Tao, S.; Design Recommendations for Bond of GFRP Rebars to Concrete, Journal of Structural Engineering; March 1996.

Greenwood, M.; Creep-Rupture Testing to Predict Long-Term Performance; CDCC 2002.

Helbling, C. and Karbhari. V.; Environmental Durability of E-Glass/Vinylester Composites Under the Combined Effect of Moisture, Temperature and Stress; Durability of FRP Composites for Construction; 192-201; 2002.

Hullat, J., Hollaway, L. and Thorne, A.; Preliminary Investigation on the Environmental Effects on new Heavyweight Fabrics for use in Civil Engineering: Composites Part B: Engineering; May 26, 2002.

Kayyali, O.; Bond Slip of Coated Reinforcement in Concrete, Construction and Building Materials, Vol. 9(4), 1995

Kowalchuk, G. S.; Brookside Cemetery Pre-cast Concrete Headstone Supports – review of the deterioration of the pre-cast concrete headstone supports; July 21, 1990.

Liao, K., Schultheisz, C.R. and Huntson; D.L.; Effects of Environmental Aging on the Properties of Pultruded GFRP; Composites: Part B: Engineering; 1998.

Lundgren, K.; Model for the Bond Between Concrete and Reinforcement, Magazine of Concrete Research, Vol. 52(1); 2000.

Melvar, L.J., Jamond, R.M., Hoffard, T.A.; and Novinson T., GFRP Composites in Simulated Marine Environments; CDCC 2002.

Mufti, A. and Onofrei, M.; Long-Term Performance of GFRP and Steel Anchor Assembly for Markers in Concrete at Veterans Affairs – Brookside Cemetery; Final Report; ISIS Canada Research Network, University of Manitoba; October 2004.

Mufti, A., Onofrei, M. and Kroeker, A.; Long-Term Performance of Anchor Assembly for Marker in Conrete at Veterans Affairs – Brookside Cemetery; Technical Report; ISIS Canada Research Network, University of Manitoba; June 2004.

Mufti, A.A., Onofrei, M. and Klowak, C.; Freeze-Thaw testing of Brookside Cemetery Marker Mounting; ISIS Canada Research Network; Technical Report; April 2003.

Mufti, A.A., Onofrei, M., Benmokrane, B., Banthia, N., Boulfiza, M., Newhook, J.P., Bakht, B., Tadros, G. and Brett, P.; Report on the Studies of GFRP Durability in Concrete From Field Demonstration Structures; Composites in Construction – Third International Conference; 2005.

Nilson, A.; Finite Element Modeling of Reinforced Concrete; Ph.D. Thesis; University of Manitoba; 1968.

Pillai, S., Kirk, D. and Erki, M.; Reinforced Concrete Design, 3rd edition; McGraw-Hill Ryerson Limited; 1999.

Public Works Government Services Canada; RPP; Heritage Conservation Service; 2003.

Rahman, A.H. and Kingsley, C.Y.; Durability of FRP Grid Reinforcement; Advanced Composite Materials in Bridges and Structures; 1996.

Rizkalla, S. and Mufti, A.; Reinforcing Concrete Structures with Fibre Reinforced Polymers; ISIS Canada Research Network; Design Manual #3; Winnipeg, Manitoba, Canada; 2001.

Rossetti, V.; Local Bond Stress-Slip Relationships of GFRP Bars Embedded in Concrete; Materials and Structures; Vol. 28(180); 1995.

Sen, R., Mullins, G. and Salem, T.; Durability of E-Glass/Vinylester Reinforcement in Alkaline Solution; American Concrete Institute Structural Journal; May-June 2002.

Stone, D.K., Koenigsfeld, D., Myers, J. and Nanni, A; Durability of GFRP Rods, Laminates, and Sandwich Panels Subjected to Various Environmental Conditioning; Durability of Fibre Reinforced Plymer Composites for Construction - CDCC,

2002.Uomoto, T. and Nishimura; T.; Deterioration of Aramid, Glass and Carbon Fibres Due to Alkali, Acid, and Water in Different Temperatures; Fibre Reinforced Polymer Reinforcements; p 515 – 521; 1999.

Weaver, M. E.; Conservation and Stabilization Study; Brookside Cemetery Winnipeg Manitoba; Report, February 2002.

APPENDIX A – SHEAR TEST STRAIN GAUGE GRAPHS

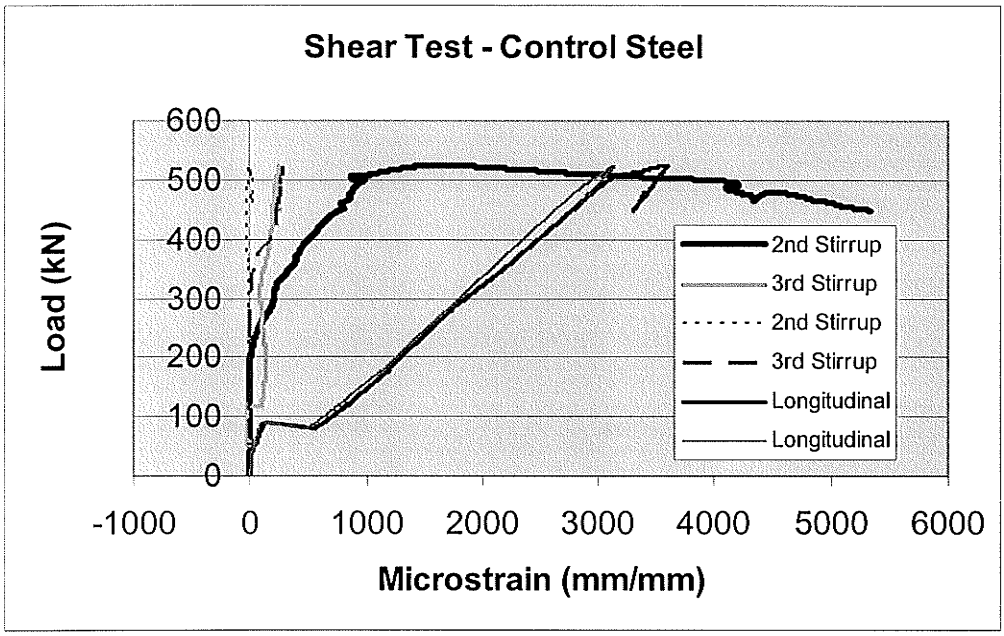

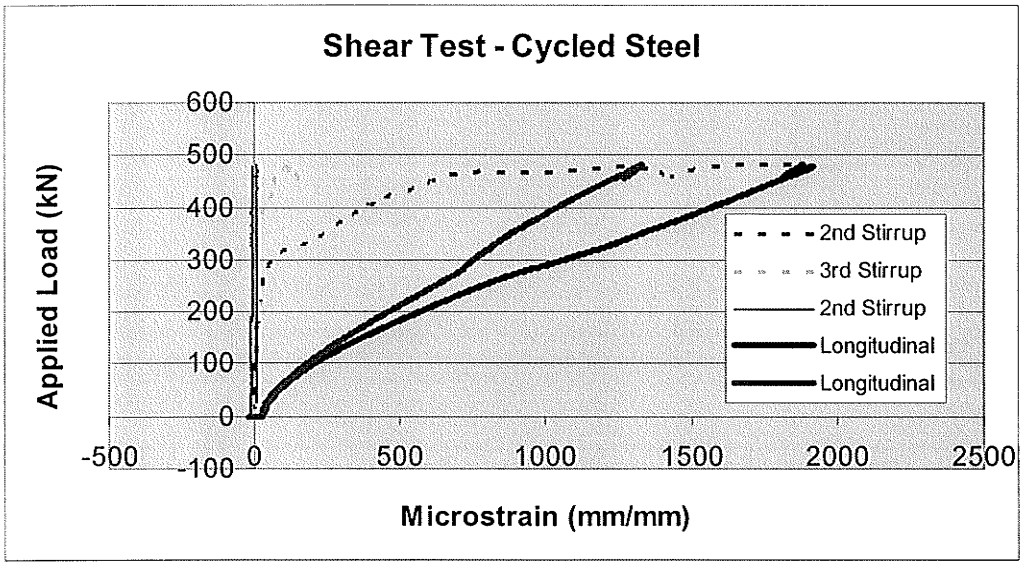

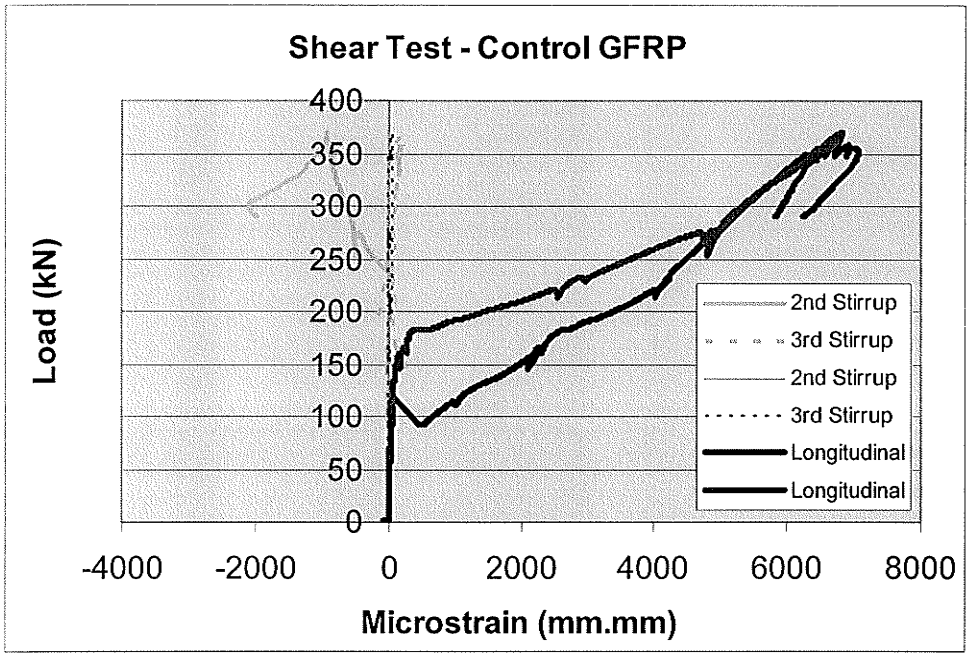
Shear Test - Control GFRP
Load (kN)
400
350
300
250
200
150
100
50
0
-4000
-2000
0
2000
4000
6000
8000
Microstrain (mm.mm)
2nd Stirrup
3rd Stirrup
2nd Stirrup
3rd Stirrup
Longitudinal
Longitudinal

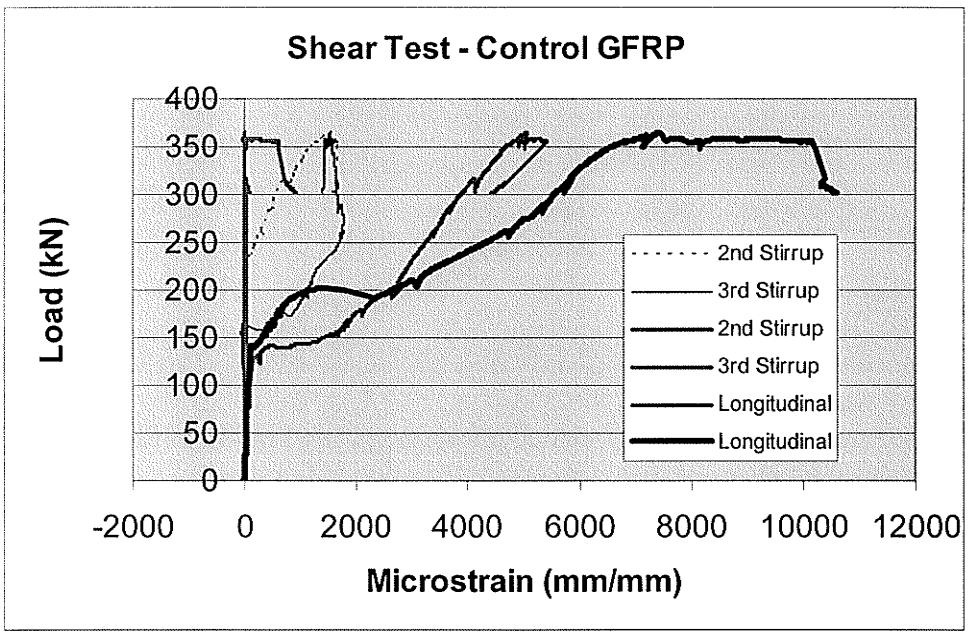
Shear Test - Control GFRP
Load (kN)
400
350
300
250
200
150
100
50
0
-2000
0
2000
4000
6000
8000
10000
12000
Microstrain (mm/mm)
2nd Stirrup
3rd Stirrup
2nd Stirrup
3rd Stirrup
Longitudinal
Longitudinal

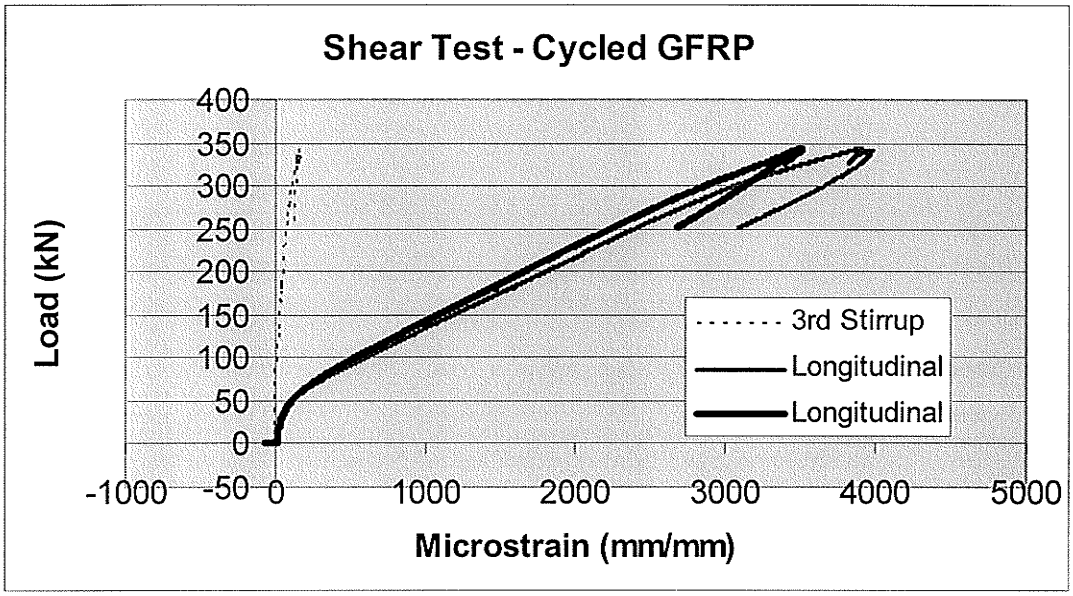
Shear Test - Cycled GFRP
Load (kN)
400
350
300
250
200
150
100
50
0
-50
-1000
0
1000
2000
3000
4000
5000
Microstrain (mm/mm)
3rd Stirrup
Longitudinal
Longitudinal

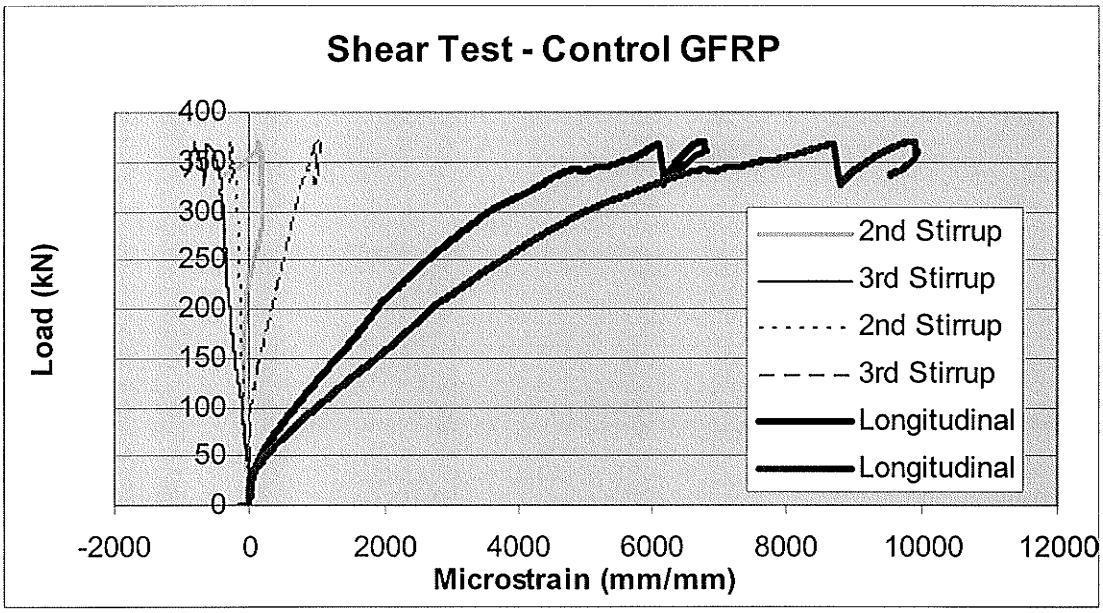
Shear Test - Control GFRP
Load (kN)
400
350
300
250
200
150
100
50
0
-2000
0
2000
4000
6000
8000
10000
12000
Microstrain (mm/mm)
2nd Stirrup
3rd Stirrup
2nd Stirrup
3rd Stirrup
Longitudinal
Longitudinal

APPENDIX B – BENDING TEST STRAIN GAUGE GRAPHS

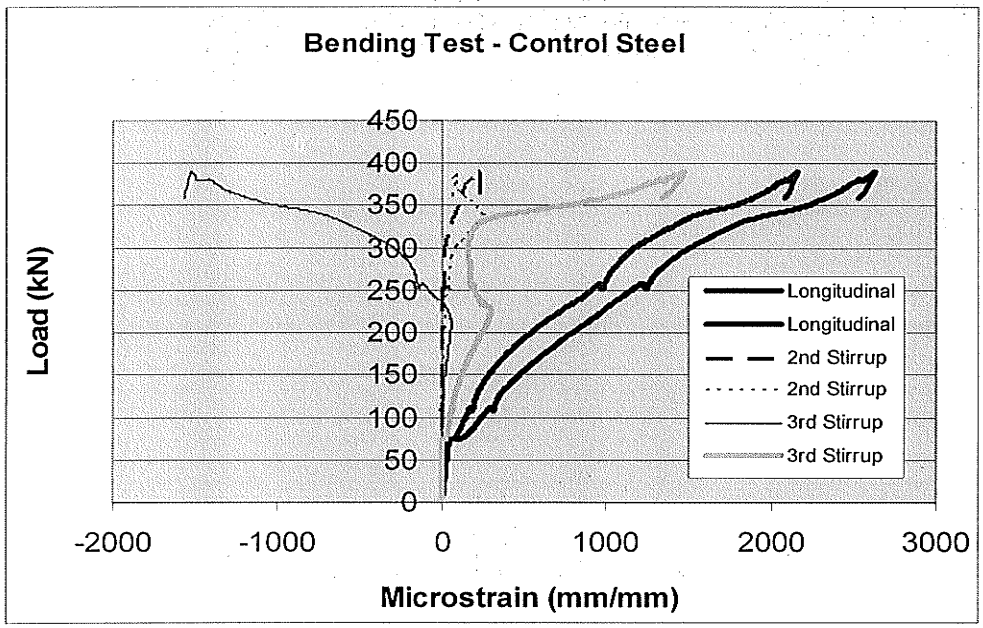

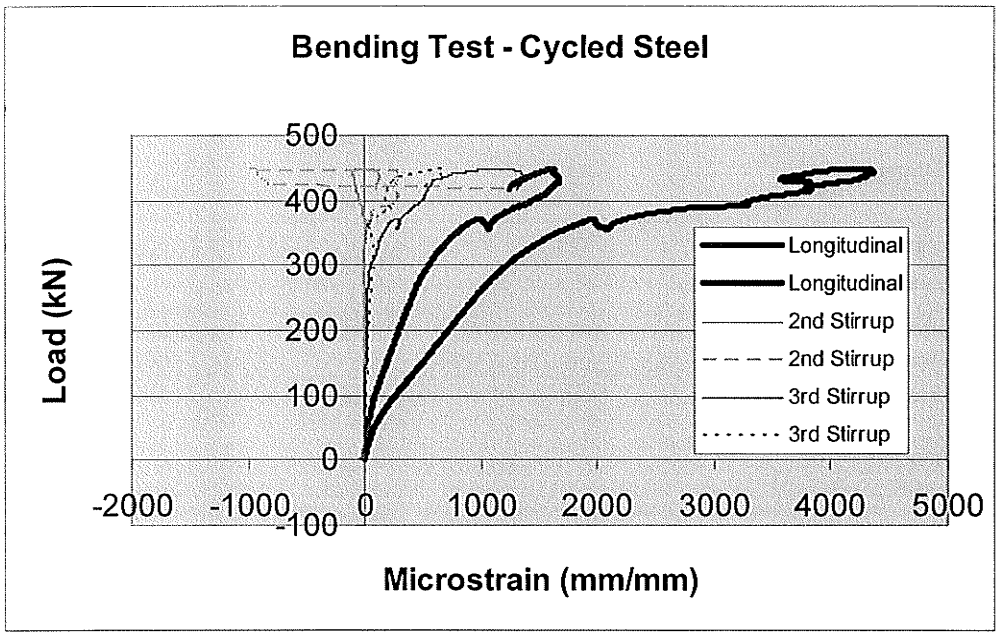

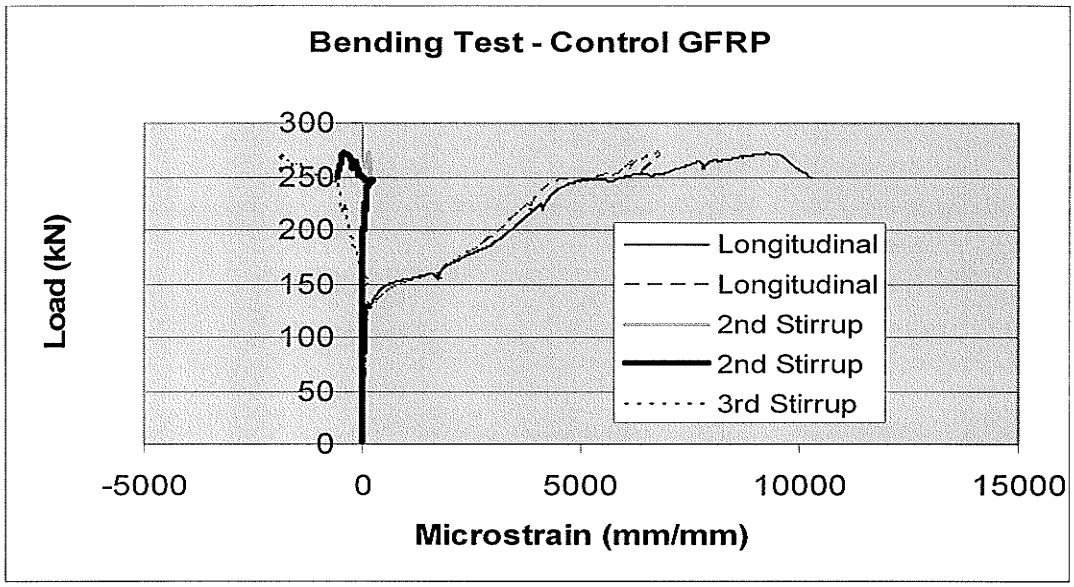
Bending Test - Control GFRP
Load (kN)
300
250
200
150
100
50
0
-5000
0
5000
10000
15000
Microstrain (mm/mm)
Longitudinal
Longitudinal
2nd Stirrup
2nd Stirrup
3rd Stirrup

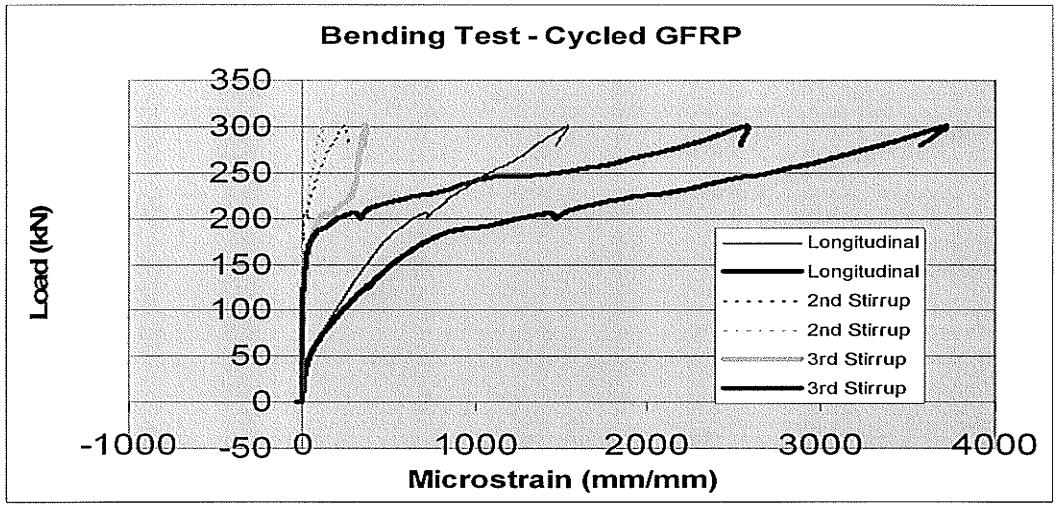
Bending Test - Cycled GFRP
Load (kN)
350
300
250
200
150
100
50
0
-1000
-50
0
1000
2000
3000
4000
Microstrain (mm/mm)
Longitudinal
Longitudinal
2nd Stirrup
2nd Stirrup
3rd Stirrup
3rd Stirrup

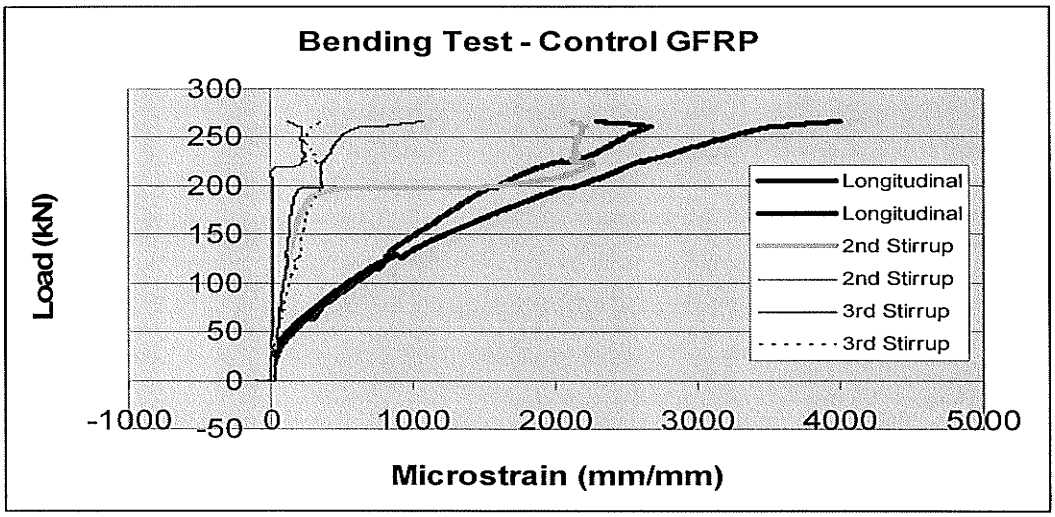
Bending Test - Control GFRP
Load (kN)
300
250
200
150
100
50
0
-1000
-50
0
1000
2000
3000
4000
5000
Microstrain (mm/mm)
Longitudinal
Longitudinal
2nd Stirrup
2nd Stirrup
3rd Stirrup
3rd Stirrup